Pseudohalide tectons within the coordination sphere of the uranyl ion: An experimental and theoretical study of C—H···O, C—H···S and chalcogenide non-covalent interactions.

*Stefano Nuzzo,[1] Brendan Twamley,[1] James A. Platts,[2] and Robert J. Baker[1]**

1 School of Chemistry, University of Dublin, Trinity College, Dublin 2, Ireland

2 School of Chemistry, Main Building, Cardiff University, Park Place, Cardiff, CF10 3AT, U.K.

ABSTRACT. A series of uranyl thiocyanate and selenocyanate of the type $[R_4N]_3[UO_2(NCS)_5]$ (R_4 = ^{n}Bu$_4$, Me$_3$Bz, Et$_3$Bz), $[Ph_4P][UO_2(NCS)_3(NO_3)]$ and $[R_4N]_3[UO_2(NCSe)_5]$ (R_4 = Me$_4$, ^{n}Pr$_4$, Et$_3$Bz) have been prepared and structurally characterized. The resulting non-covalent interactions have been examined and compared to other examples in the literature. The nature of these interactions is determined by the cation so that when the alkyl groups are small, chalcogenide···chalcogenide interactions are present, but this 'switches off' when R = ^{n}Pr and charge assisted U=O···H—C and S(e)···H—C hydrogen bonding remain the dominant interaction. Increasing the size of the chain to ^{n}Bu results in only S···H—C interactions. Spectroscopic implications of these chalcogenide interactions have been explored in the vibrational and photophysical properties of the series $[R_4N]_3[UO_2(NCS)_5]$ (R_4 =Me$_4$, Et$_4$, ^{n}Pr$_4$, ^{n}Bu$_4$, Me$_3$Bz, Et$_3$Bz), $[R_4N]_3[UO_2(NCSe)_5]$ (R_4 = Me$_4$, ^{n}Pr$_4$, Et$_3$Bz) and $[Et_4N]_4[UO_2(NCSe)_5][NCSe]$. The data suggest that U=O···H—C interactions are weak and do not perturb the uranyl moiety. While the chalcogenide interactions do not influence the photophysical properties, a coupling of the U=O and δ(NCS) or δ(NCSe) vibrational modes is observed in the 77K solid state emission spectra. A theoretical examination of representative examples of Se···Se, C—H···Se and C—H···O=U by molecular electrostatic potentials, NBO and AIM methodologies give a deeper understanding of these weak interactions. C—H···Se are individually weak but C—H···O=U interactions are even weaker supporting the idea that the –yl oxo's are weak Lewis bases. An Atoms in Molecules study suggest that the chalcogenide interaction is similar to lone pair…π or fluorine…fluorine interactions. An oxidation of the NCS ligands to form $[(UO_2)(SO_4)_2(H_2O)_4].3H_2O$ was also noted.

KEYWORDS: Non-covalent interactions; uranyl chemistry; photoluminescence; AIM

Introduction

An understanding of the plethora of non-covalent interactions is of importance, not just in structural chemistry but also materials and biological chemistry. While the hydrogen bond is the most well studied, over the past few years other non-conventional noncovalent interactions have garnered significant amount of attention, such as halogen bonding,[1] pnictogen bonding,[2] and even aerogen bonding.[3] Chalcogenide bonding[4] is a relatively recent addition to the toolbox of crystal engineering and follows the same type of bonding scheme as halogen bonding, namely a σ-hole.[5] This bonding scheme can be viewed comparably to hydrogen bonding as X—D···A, where X is any atom, D is the donor atom and A is the acceptor atom. The σ-hole is visualized as a region of positive electrostatic potential found on an empty σ* orbital and is dependent upon two parameters: the σ-hole becomes more positive (and hence stronger interactions) when (1) D is more polarizable and (2) when the X atom is more electron withdrawing. The majority of chalcogenide bonding features attractive interactions between S or Se and an electronegative N or O donor. Computational studies on Se···O or S···N interactions have recently been conducted and shown them to be dependent on the substituents on the selenium atom and the interactions described as a charge transfer from the N lone pair to the σ* Se—X orbital (Chart 1).[4j,6] Synthetic molecular balances based on formamide and thioformamide units have confirmed this, and shown that chalcogenide…H—C interactions can also be described in this manner.[4b] The atomic polarizability increases down the group so that S = 19.3 a.u. and Se 25.4 a.u. (a.u. = atomic units); thus a stronger interaction should occur when descending the group.[7] Moreover, as the atomic radius increases steric effects become less pronounced as the group is descended. These interactions can be comparable in strength to hydrogen and halogen bonding. For example, the computed interaction energy of $FHS\cdots NH_3$ is -8.4 kcal mol^{-1} compared to -11.3 kcal mol^{-1} for $FHSe\cdots NH_3$ and -10.3 kcal

mol^{-1} for the halogen bonded F—Cl···NH_3.[5d] Perhaps more illuminating is the low temperature structure of the F_4S···NEt_4 adduct which displays an S—N bond length of 2.384(2) Å, typical for a dative covalent bond;[8] theory supports this hypothesis[9] and reports a binding energy of -14.4 kcal mol^{-1}.

Halogen interactions have been further delineated by the geometric parameters shown in Chart 1. $0^o \leq |\theta_1 - \theta_2| \leq 15^o$ are classified as type I; $15^o \leq |\theta_1 - \theta_2| \leq 30^o$ are quasi-type I/type II and $30^o \leq |\theta_1 - \theta_2|$ are type II.[10] Type I are generally thought to be due to crystal packing, while Type II are stabilizing interactions. A recent examination of the Cambridge database showed that the majority of S···S interactions in sp^2 hybridized sulfur are Type I ($\theta_1 \approx \theta_2$).[11] It is also apparent that S···O interactions are prevalent in molecular recognition and host-guest interactions in biological systems.[12] However few examples of chalcogenide interactions exist where a metal ion is included.[13] Indeed, even the more mature field of halogen bonding features limited examples, notably iodoform adducts of trans-[$PtX_2(NCNR_2)_2$],[14] or in a uranyl organic framework based on halogen substituted isonicotinic acids.[15]

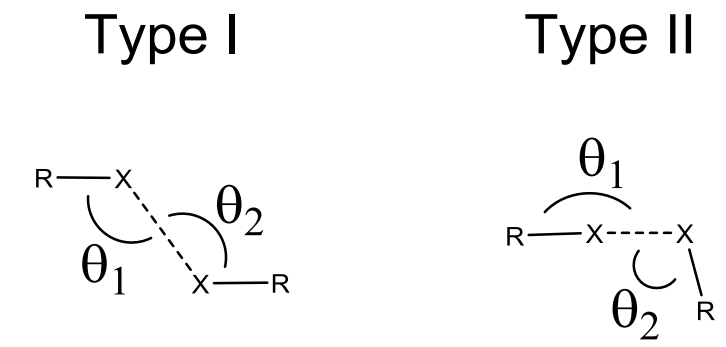

Chart 1. Types of halogen and chalcogenide bonding.

The uranyl ion has a number of features that make it attractive for a study on non-covalent interactions. The coordination geometry is generally limited by the linear O=U=O (–yl) fragment so all coordination will be directed to the equatorial plane.[16] Changing the equatorial ligands can influence the properties of the uranyl ion in catalytic applications[17] or the formation of uranyl coordination polymers with great effect.[18] Over the last few years the –yl moiety has been shown to act as a secondary directing influence in supramolecular assembly to form 3-dimensional structures. However, as the oxo groups are generally considered as poor Lewis bases these interactions have been somewhat neglected. Interactions with metal cations can elongate the U=O bond length to a degree that is noticeable crystallographically.[19] Some evidence suggests that this weakening of the U=O bond is due to the increase in electron density around the uranyl cation and increase electrostatic repulsions within the U=O group.[20] For weaker interactions, hydrogen bonding acceptor via C—H···O=U interactions,[21] sometimes via charge assisted hydrogen bonding,[22] can be used to recognize or separate the uranyl ion selectively from complex mixtures.[23] More recently, the uranyl ion as a halogen bond acceptor[24] has been observed. Finally, additional supramolecular interactions utilizing the equatorial ligands as tectons have been utilized. For example, the elegant studies using uranyl thiocyanate to explore non-covalent bonding in halogenated pyridinium cations showed some evidence for S···S close contacts.[25] In relation to this we recently reported close contacts between two selenium atoms in $[Et_4N]_4[UO_2(NCSe)_5][NCSe]$ ($d_{Se...Se}$ = 3.427(1) Å).[26] A series of $[R_4N]_3[UO_2(NCS)_5]$ (R = Me, Et, ^{n}Pr)[27] have been structurally characterized as examples of species present in spent nuclear fuel reprocessing. Moreover, the uranyl thiocyanate ion has shown to have unusual thermochromic behavior in ionic liquids.[28]

In this contribution we have extended our study of the coordination chemistry of the $[NCSe]^-$ pseudohalide as a tecton in uranyl coordination chemistry, of which there is only one other

example.[29] We also compare the uranyl selenocyanate chemistry to that of uranyl thiocyanate compounds which we[30] and others[27] have reported, and explore the other non-covalent interactions, namely charge assisted C—H···O=U and C—H···S(e) hydrogen bonding interactions. To do this we have utilized X-ray crystallography, vibrational and photoluminescence spectroscopy and theoretical methods to further our understanding of these weak interactions.

Results and Discussion

Synthesis and Structural studies.

The syntheses of all the compounds described herein are simple (Equations 1 and 2) and X-ray quality crystals grown for all. We will use the nomenclature RE, where R is the alkyl group of the ammonium cation and E is S or Se to distinguish these compounds. Thus we have a small library of compounds that we can compare structural parameters and packing motifs (i) within the NCS series, (ii) within the NCSe series and (iii) with the same cations. In one case we also obtained a small amount of a decomposition product presumably from $[NCS]^-$ oxidation and this has been structurally characterized. When the reaction of cyanates were examined, we consistently observed hydrolysis of the $[NCO]^-$ fragment and $K_4[UO_2(CO_3)_3]$ the only product obtained. In contrast, the reaction of $[NCTe]^-$ with uranyl nitrate afforded immediate decomposition to a grey precipitate of presumably tellurium metal and, from the acetonitrile soluble fraction, single crystals of $[Et_4N]_2[UO_2Cl_4]$ were deposited. $[NCTe]^-$ chemistry is dominated by this decomposition.[31]

$$[UO_2(NO_3)_2].6H_2O + 5\ NaNCS + 3R_4NCl \rightarrow [R_4N]_3[UO_2(NCS)_5] \quad (1)$$

$$[UO_2(NO_3)_2].6H_2O + 5\ KNCSe + 3R_4NCl \rightarrow [R_4N]_3[UO_2(NCSe)_5] \quad (2)$$

(i) $[R_4N]_3[UO_2(NCS)_5]$ series (R = Me, Et, ^{n}Pr, ^{n}Bu, Me_3NBz, Et_3NBz)

The solid-state structures of MeS, EtS and ^{n}PrS have been previously described,[27] but the focus of that work was not on the supramolecular structures, whereas ^{n}BuS, Me_3NBzS and Et_3NBzS are new. An example of the structure of Me_3NBzS is shown in Figure 1, while selected metric parameters for the RS series are reported in Table 1; other structural data are collated in Figure S1-S3 and Tables S1-S8. In all compounds the uranyl geometry is, as expected, pentagonal bipyramidal with a linear O=U=O moiety, and the U—N, N=C and C=S bond lengths are statistically identical. The only differences are in the orientation of how the $[NCS]^-$ ion coordinates to the uranium; in particular the U—N=C angle and the deviation of the S atoms out of the UN_5 plane, which diverges significantly.

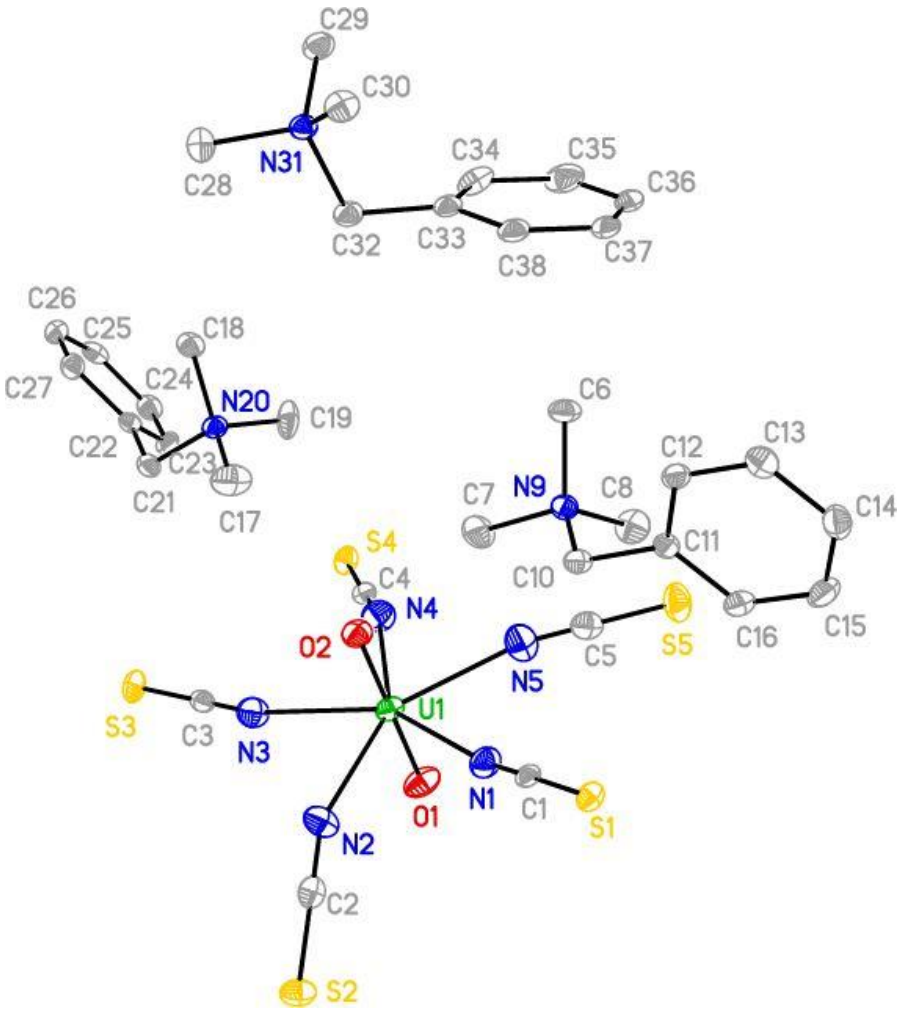

Figure 1. Asymmetric unit of Me_3NBzS with atomic displacement parameters shown at 50% probability. Hydrogen atoms omitted for clarity.

Table 1. Selected average bond lengths (Å) and angles (°) for the RS series.

Compound	U=O	U—N	N=C	C=S	O=U=O	U—N=C	S o.o.p (Å)[a]
MeS[b]	1.770(4)	2.45(2)	1.15(2)	1.62(1)	179.7(1)	154.1(4) to 176.2(4)	S1 -0.343 S2 +1.100 S3 -0.910 S4 +0.394 S5 +0.181
EtS[b]	1.763(6)	2.45(2)	1.16(1)	1.62(3)	177.4(3) 178.3(4)	155.3(7) to 176.4(7)	S1 +0.260 S2 +0.072 S3 -0.625 S4 -1.042 S5 -0.702
^{n}PrS[b]	1.749(4)	2.44(2)	1.14(1)	1.62(3)	178.9(3)	158.4(6) to 179.6(8)	S1 -0.286 S2 -0.475 S3 -0.683 S4 +0.574 S5 +0.103
^{n}BuS	1.769(10) 1.759(9)	2.45(1)	1.16(1)	1.63(1)	179.4(9)	168.6(2) to 172.3(2)	S1 -0.479 S2 -0.364 S2A -0.364 S3A -0.474
Me_3NBz	1.778(3) 1.774(3)	2.45(1)	1.16(1)	1.62(1)	179.21(13)	153.2(3) to 167.2(3)	S1 -0.797 S2 -1.404 S3 -0.087 S4 -0.760 S5 -0.708

Et_3NBz	1.772(2) 1.773(2)	2.45(1)	1.16(1)	1.63(1)	179.4(9)	168.9(3) to 172.6(3)	S1 +0.466 S2 +0.307 S3 -0.219 S4 -0.342 S5 +0.296

a distance out of the UN_5 plane.

b from Reference 27

Apparent in the structures of MeS and EtS are S···S close contacts within the van der Waals radii for two S atoms (3.78 Å).[32] In MeS these are Type I interactions ($d_{S\cdots S}$ = 3.587 Å, θ_2-θ_1 = 0°). In contrast, EtS forms chains along the crystallographic *b*-axis and the angles θ_1 and θ_2 suggest these are not crystal packing (Figure 2a), in accord with the conventional description for halogen bonding (Chart 1); we believe that this is applicable here as the interactions are both of a σ-hole type. The S···S distances and angles are: $d_{S\cdots S}$ = 3.470 Å, θ_2-θ_1 = 38.3° and $d_{S\cdots S}$ = 3.591 Å, θ_2-θ_1 = 20.8°. There are also S···H—C weak hydrogen bonds[33] ($d_{S\cdots C}$ = 3.540(8) to 3.895(7) Å) where the alkylammonium cation links two chains. It appears that the S···H—C interaction is responsible for the movement of the sulfur atom out of the UN_5 plane. Also present are longer C—H···O=U hydrogen bonds ($d_{O\cdots C}$ = 3.21 and 3.47 Å). As the size of the R group increases the close contacts between two S centers are no longer present, and in the ^{n}Pr case, S···H—C interactions are prevalent (Figure 2b; $d_{S\cdots C}$ = 3.74 – 3.84 Å) along with bifurcated hydrogen bonding to the uranyl ion ($d_{O\cdots C}$ = 3.40 and 3.49 Å). We have prepared and structurally characterized ^{n}BuS and there are no S···S close contacts. Thus it appears that there is a steric effect of the cation in the nature of these non-covalent interactions, whereby the conformationally non-rigid arms of the n-propyl chain are enough to 'turn-off' the S···S close contacts, while the S···H—C interactions dominate all

structures. Support for this hypothesis comes from the structures of $[Me_3NBz]_3[UO_2(NCS)_5]$ and $[Et_3NBz]_3[UO_2(NCS)_5]$ where there are short contacts between two sulfur atoms, but the angles suggest a type I interaction, *i.e.* due simply to packing (Me_3NBzS: $d_{S\cdots S}$ = 3.350 Å, θ_2-θ_1 = 0°; Et_3NBzS: $d_{S\cdots S}$ = 3.540 Å, θ_2-θ_1 = 14.0°). However, these systems enable us to explore the C—H···S interactions in more detail (Me_3NBzS: $d_{S\cdots C}$ = 3.690(3) to 3.824(3) Å; Et_3NBzS: $d_{S\cdots C}$ = 3.711(4) to 3.849(5) Å). It has been reported from computational studies that the strength of this weak hydrogen bond is dependent upon the hybridization of the C—H donor and this decreases as hybridization increases,[34] but in the structures of Me_3NBzS and Et_3NBzS there is no obvious correlation. From this description it is clear that the supramolecular structures are influenced subtly by the steric effects of the cation.

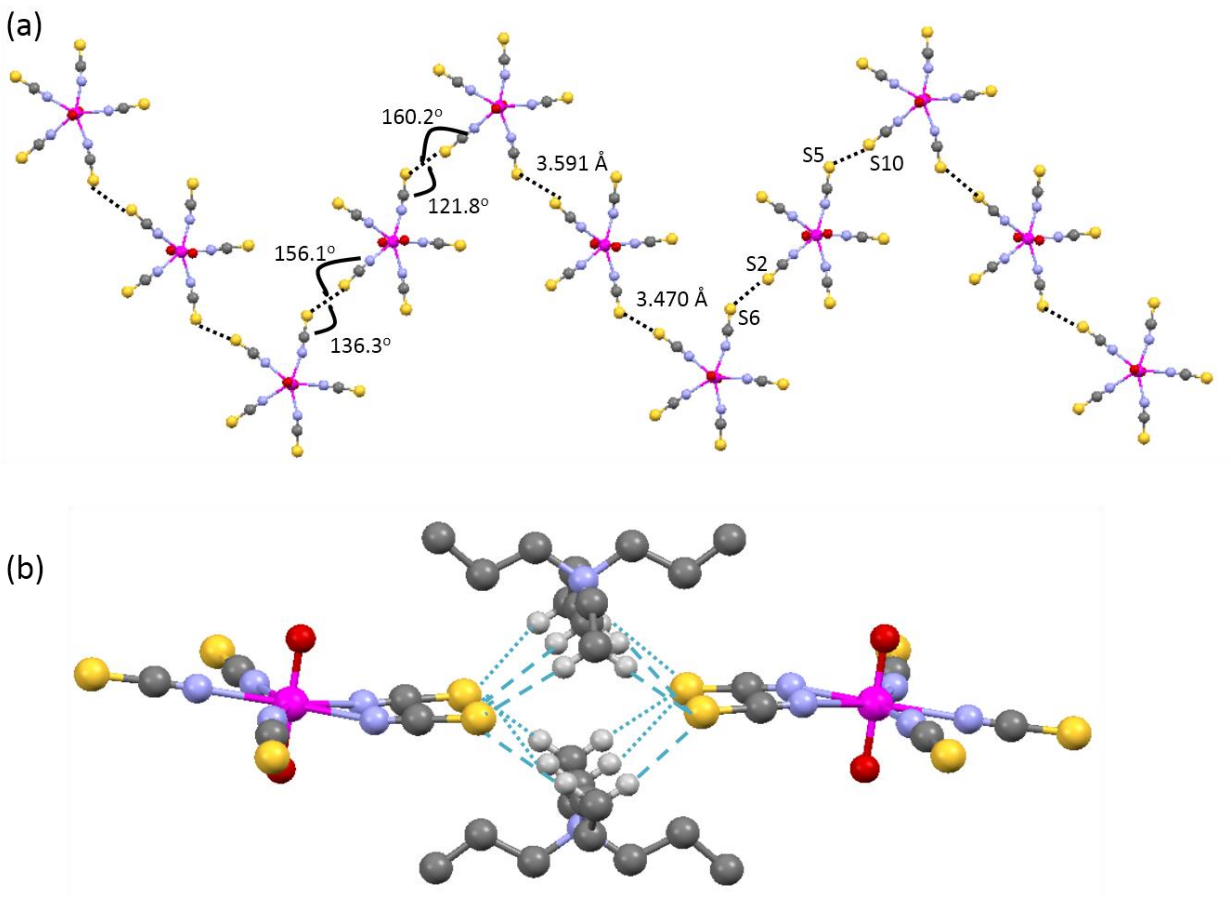

Figure 2. Supramolecular structure of (a) EtS highlighting the non-covalent S···S interactions (black lines) and (b) the S···H-C hydrogen bonding in ^{n}PrS (blue lines). Color code: U – pink; O – red; N- blue; C – grey; S – yellow; H – white.

A further secondary interaction occurs between the C—H of the cation and the uranyl group. The –yl oxo is well known to act as a hydrogen bond acceptor.[21,22] In all the examples in this series, except for ^{n}BuS, there are numerous short contacts with $d_{C\cdots O}$ between 3.0-3.5 Å; Figure 3 shows a specific example. These hydrogen bonding interactions do not perturb the U=O bond lengths, as

all examples are essentially identical to that of BuS which does not feature any U=O···H—C close contacts, indicating that the hydrogen bonding interactions are very weak (*vide infra*).

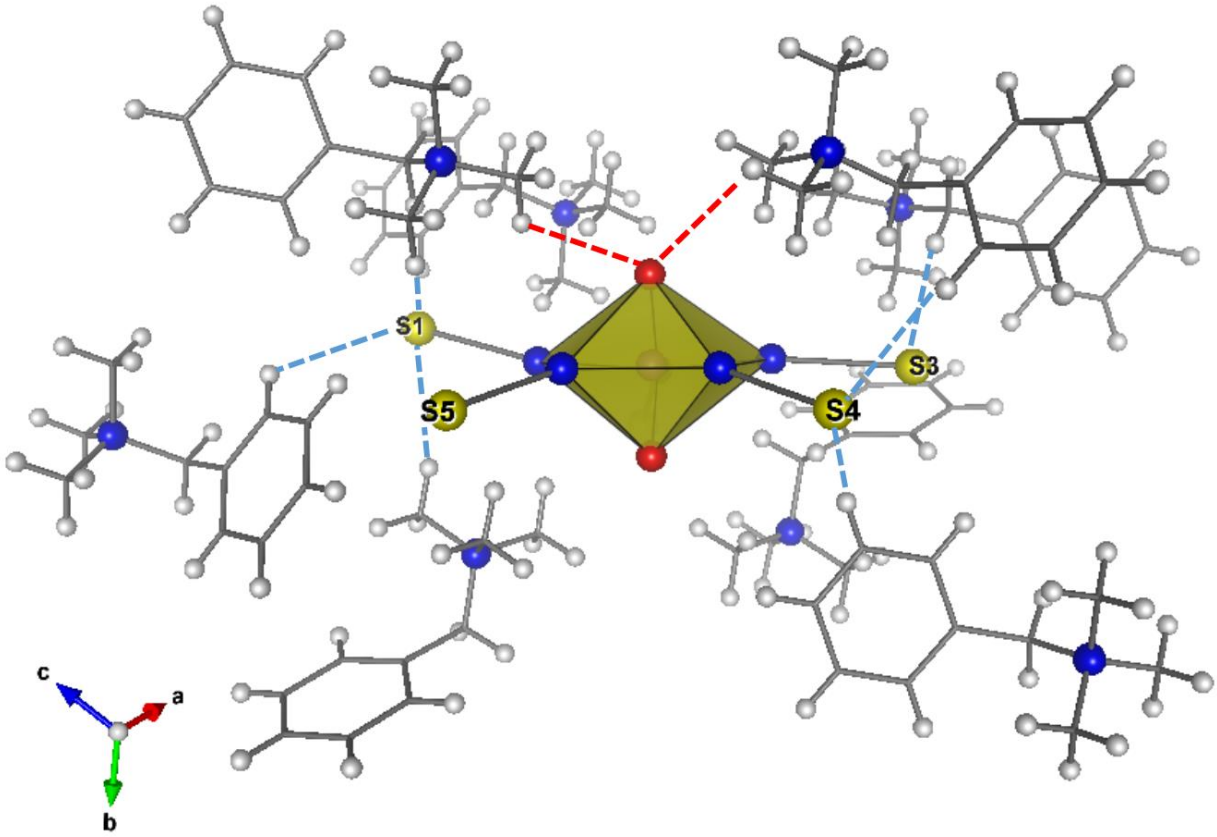

Figure 3. Supramolecular interactions in Me_3NBzS: dashed red line U=O···H—C and dashed blue line S···H—C.

During one attempt at the synthesis of $[Ph_4P]_3[UO_2(NCS)_5]$ we obtained a few single crystals that were shown to be $[Ph_4P]_2[UO_2(NCS)_3(NO_3)]$ by single crystal X-ray diffraction. We were able to increase the yield using the correct stoichiometry, albeit as a polymorph, but have been unable to

crystallize the homoleptic thiocyanate complex with this cation. The structure of this compound is shown in Figure 4. The bond lengths are similar to the homoleptic series described above, with the exception that the U-N bond lengths are slightly shorter (2.412(8) and 2.402(11) Å). The U—O bond length (2.503(7) Å) is typical for a nitrate ion coordinated in a bidentate fashion. There are no S···S close contacts in this case and the dominant interactions are C—H···O hydrogen bonding to the nitrate ion ($d_{C\cdots O}$ = 3.237(10) Å) and longer C—H···S ($d_{C\cdots S}$ = 3.736(9) Å); the $[NCS]^-$ ion involved in this interaction is bent out of the UN_5 plane (0.307 Å; C(1)-N(1)-U(1) = 166.2(7)°) in comparison to that $[NCS]^-$ ion that does not have close contacts which is in the plane (C(2)-N(2)-U(1) = 180.0°), adding weight to our thesis that it is the weak hydrogen bonding that is responsible for the disruption in the U—NCS coordination environment.

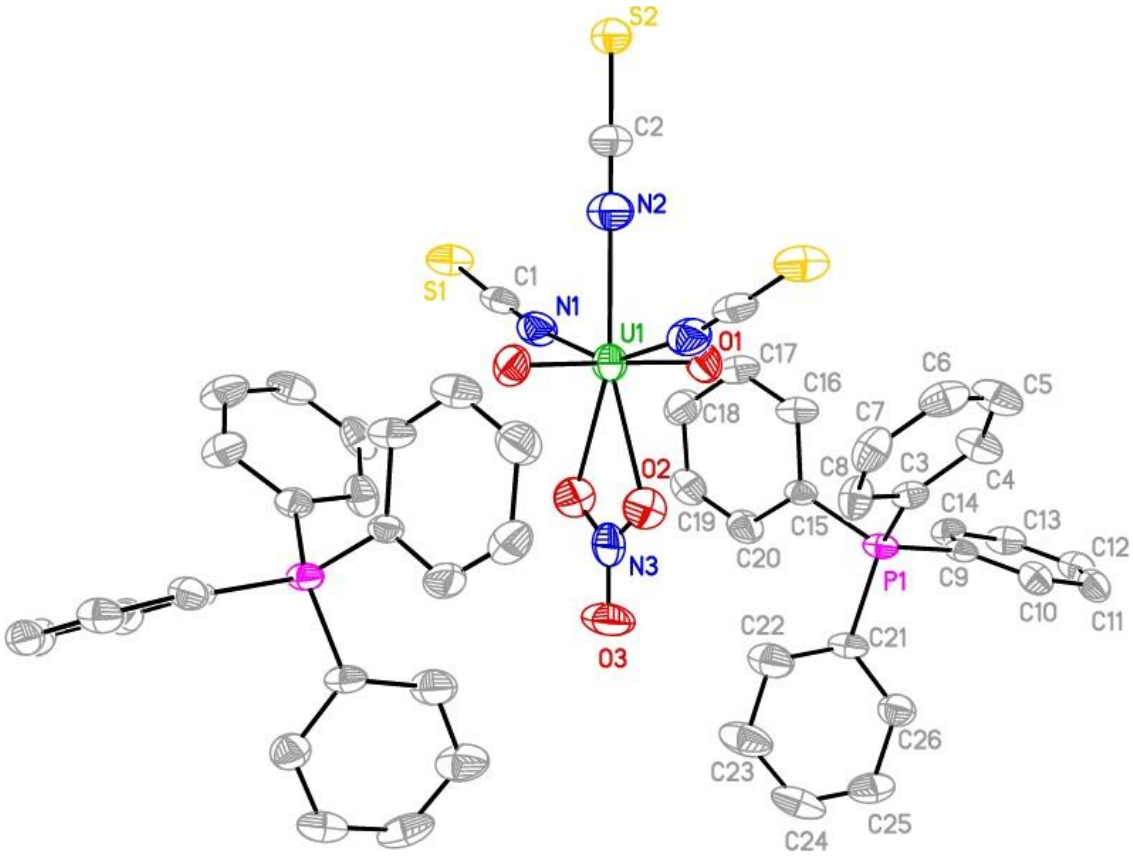

Figure 4. Molecular structure of $[Ph_4P]_2[UO_2(NCS)_3(NO_3)]$ with atomic displacement parameters shown at 50% probability. Hydrogen atoms omitted for clarity. Symmetry unique atoms labelled only.

In an attempted reaction of uranyl nitrate, sodium thiocyanate and Me_3SnCl, we did not isolate the expected species, but instead structurally characterized $[(UO_2)_2(SO_4)_2(H_2O)_4].3H_2O$. The mechanism of oxidation of the $[NCS]^-$ ion is not immediately apparent, but there is some literature precedent for oxidation of coordinated thiocyanate to sulfate.[35] Nevertheless the structure is α-uranyl sulfate determined in 1978,[36] and similar to the mineral Shumwayite,[37] $[(UO_2)_2(SO_4)_2].5H_2O$. Our refinement is significantly better so we have included it herein but will not comment further.

(ii) $[R_4N]_3[UO_2(NCSe)_5]$ series (R = Me, Et, ^{n}Pr, Et_3NBz)

The number of structurally characterized uranyl selenocyanate compounds numbers only two: we reported the structural characterization of $[Et_4N]_4[UO_2(NCSe)_5][NCSe]$,[26] and Walensky and co-workers reported a tridentate salicylaldiminate uranyl complex of $[NCSe]^-$.[29] We have extended our initial study to include $[Me_4N]_3[UO_2(NCSe)_5].H_2O$ (MeSe), ^{n}PrSe and Et_3NBzSe, all of which have been structurally characterized. The gross solid-state structures are the same as for the RS series, and an exemplar, ^{n}PrSe, is shown in Figure 5, while the other structures are in Figures S4-S6. The pertinent metric parameters are collated in Table 2 and Tables S9-S14, and there are no significant differences in the series.

Table 2. Selected average bond lengths (Å) and angles (°) for the RSe series.

Compound	U=O	U—N	N=C	C=Se	O=U=O	U—N=C	Se o.o.p[a]
MeSe	1.769(5) 1.763(5) 1.768(5) 1.764(5)	2.46(2)	1.15(3)	1.80(3)	179.0(3) 178.7(3)	162.0(6) to 179.0(7)	Se1 +0.609 Se2 +0.710 Se3 +0.114 Se4 +0.227 Se5A +1.552 Se5B +1.879 Se6 -1.145 Se7 +0.135 Se8 +0.249 Se9 -0.073 Se10 +0.018
EtSe[a]	1.771(2)	2.46(1)	1.15(1)	1.79(1)	179.57(9)	171.0(2) to 177.6(3)	Se1 -0.164 Se2 +0.482 Se3 -0.258 Se4 +0.496 Se5 -0.481
^{n}PrSe	1.7632(19) 1.7690(19)	2.46(1)	1.15(1)	1.78(1)	179.48(10)	157.1(2) to 173.8(2)	Se1 +0.329 Se2 -0.673 Se3 -0.035 Se4 -0.638 Se5 -0.498

Et_3NBzSe	1.765(5) 1.756(5)	2.45(2)	1.14(3)	1.79(3)	179.5(3)	167.3(7) to 174.9(7)	Se1 +0.232 Se2 +0.499 Se3 +0.203 Se4 -0.158 Se5 -0.267

a distance out of the UN_5 plane.

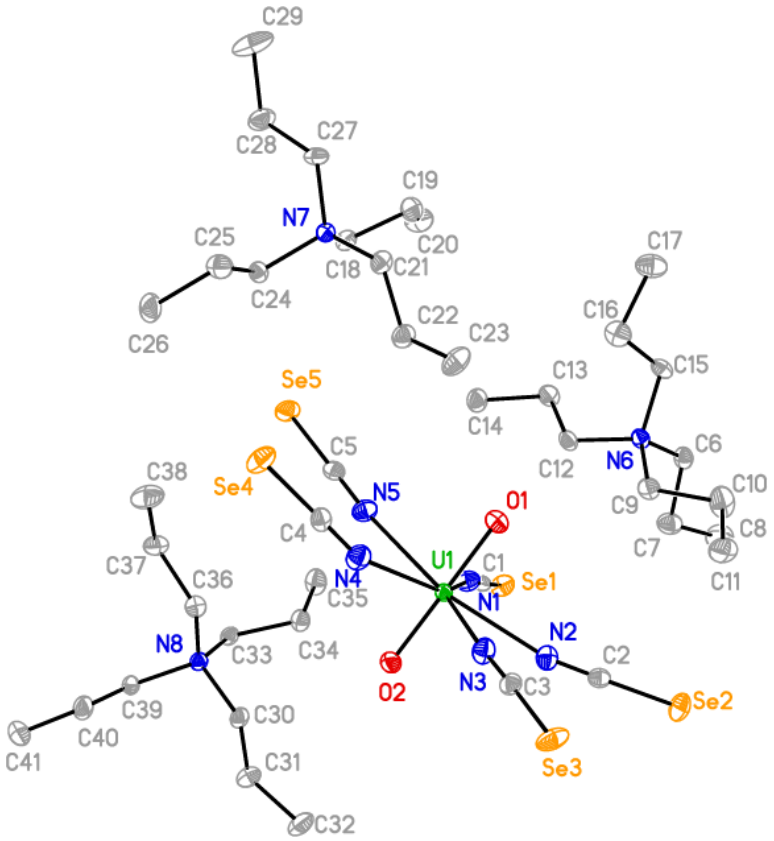

Figure 5. Molecular structure of ^{n}PrSe with atomic displacement parameters shown at 50% probability. Hydrogen atoms omitted for clarity.

The supramolecular interactions in the RSe series are greater and more complex than the RS series; in particular Se···Se interactions closer than the sum of the van der Waals radii (3.64 Å)[32] are preponderant, as expected if the bonding is via a σ-hole type mechanism. Se···H—C interactions[38] and U=O···H—C weak hydrogen bonds are also prevalent.

The packing of MeSe is shown in Figure 6. There are a number of Se···Se distances which are all slightly longer than the van der Waals radii ($d_{Se\cdots Se}$ = 3.671(2) - 3.755(3) Å), but theory shows that these are stabilizing interactions (*vide infra*). Interestingly Se(1)···Se(7), Se(4)···Se(8) and Se(3)···Se(9) form 1D sheets along the *c*-direction (Figure 6b), with C—H···Se weak hydrogen bonds ($d_{C\cdots Se}$ = 3.75 – 4.07 Å) linking the layers. C—H···O=U hydrogen bonding ($d_{C\cdots O}$ = 3.35 and 3.57 Å) interactions are also present, along with hydrogen bonding from the free water to U=O ($d_{O\cdots O}$ = 3.13 Å) and Se ($d_{O\cdots Se}$ = 3.79 Å). The water presumably comes adventitiously from the recrystallization process; notably all other compounds were prepared and recrystallized in air so it may be that the small cation allows for the inclusion of water in this case. Irrespective of the source of the water, it clearly engages in hydrogen bonding to the preference of C—H···O=U hydrogen bonding and possibly chalcogenide bonding.

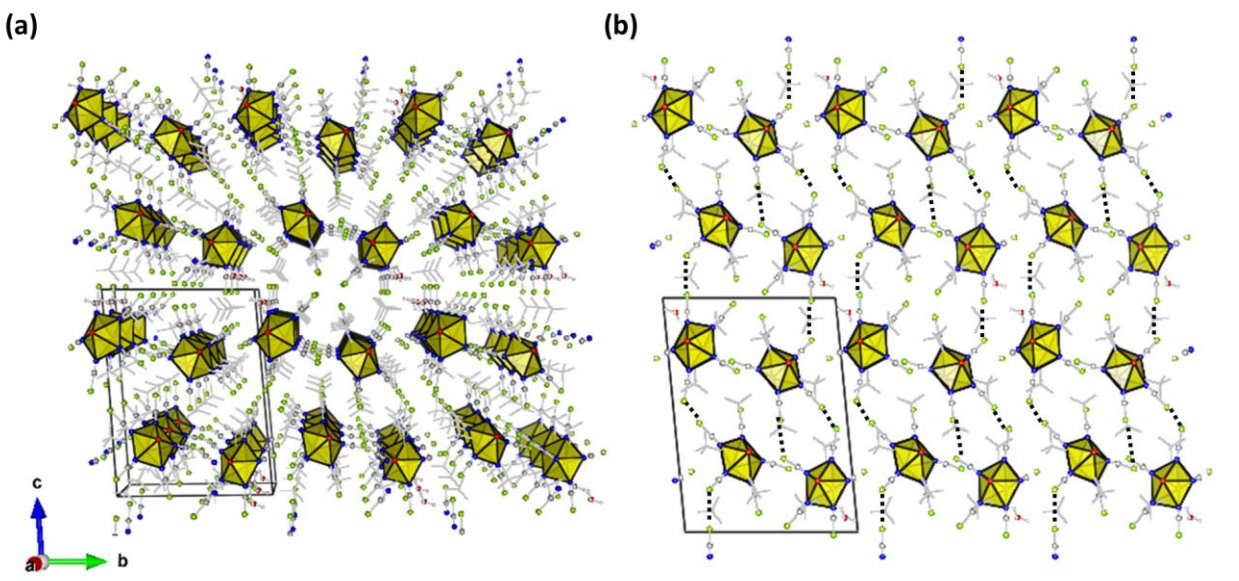

Figure 6. Packing of MeSe along the crystallographic *a*-axis. (a) A perspective view and (b) a view highlighting the Se···Se interactions (black lines).

^{n}PrSe shows no Se···Se interactions, probably due to the steric effect of the longer n-propyl arms that completely shield the uranyl complex, as illustrated in the space-filling structure (Figure 7). There are a plethora of Se···H—C ($d_{C\cdots Se}$ = 3.64 to 4.00 Å) and C—H···O=U ($d_{C\cdots U}$ = 3.175(3), 3.271(3) and 3.387(3) Å) close contacts that link the uranyl ions in layers. As in the previous series, it appears that Se···H—C interactions bend Se out of the UN_5 plane.

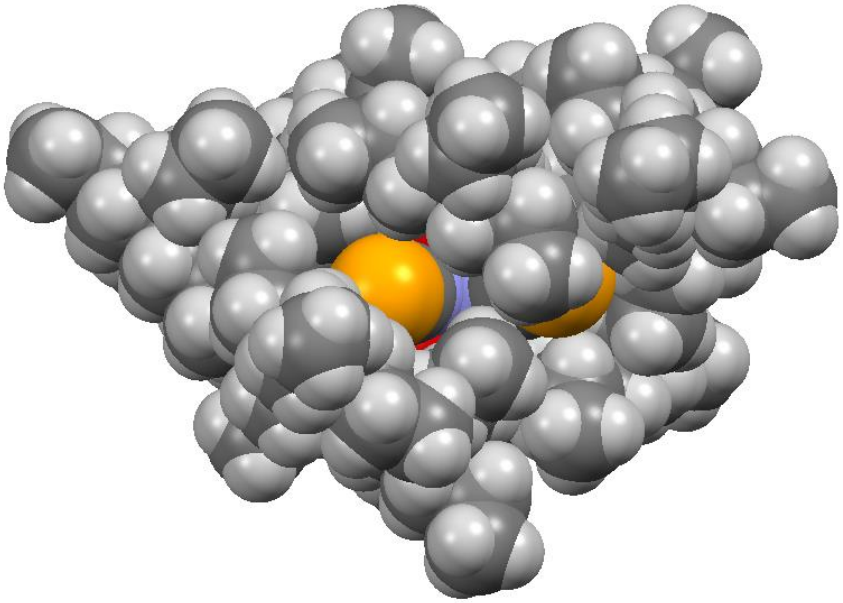

Figure 7. Space-filling view of ^{n}PrSe (orange – Se; blue – N, dark Grey – C; light gray – H; red – O; uranyl axis is parallel to the page).

In Et_3NBzSe (Figure 8) there are a number of Se···Se close contacts ($d_{Se\cdots Se}$ = 3.565(2) Å, θ_2-θ_1 = 20.7°; $d_{Se\cdots Se}$ = 3.665(2) Å, θ_2-θ_1 = 66.1°). There are also multiple Se..H—C ($d_{C\cdots Se}$ = 3.790(8) - 3.913(8) Å) and U=O···H—C ($d_{C\cdots U}$ = 3.310(9) - 3.59(1) Å) interactions present.

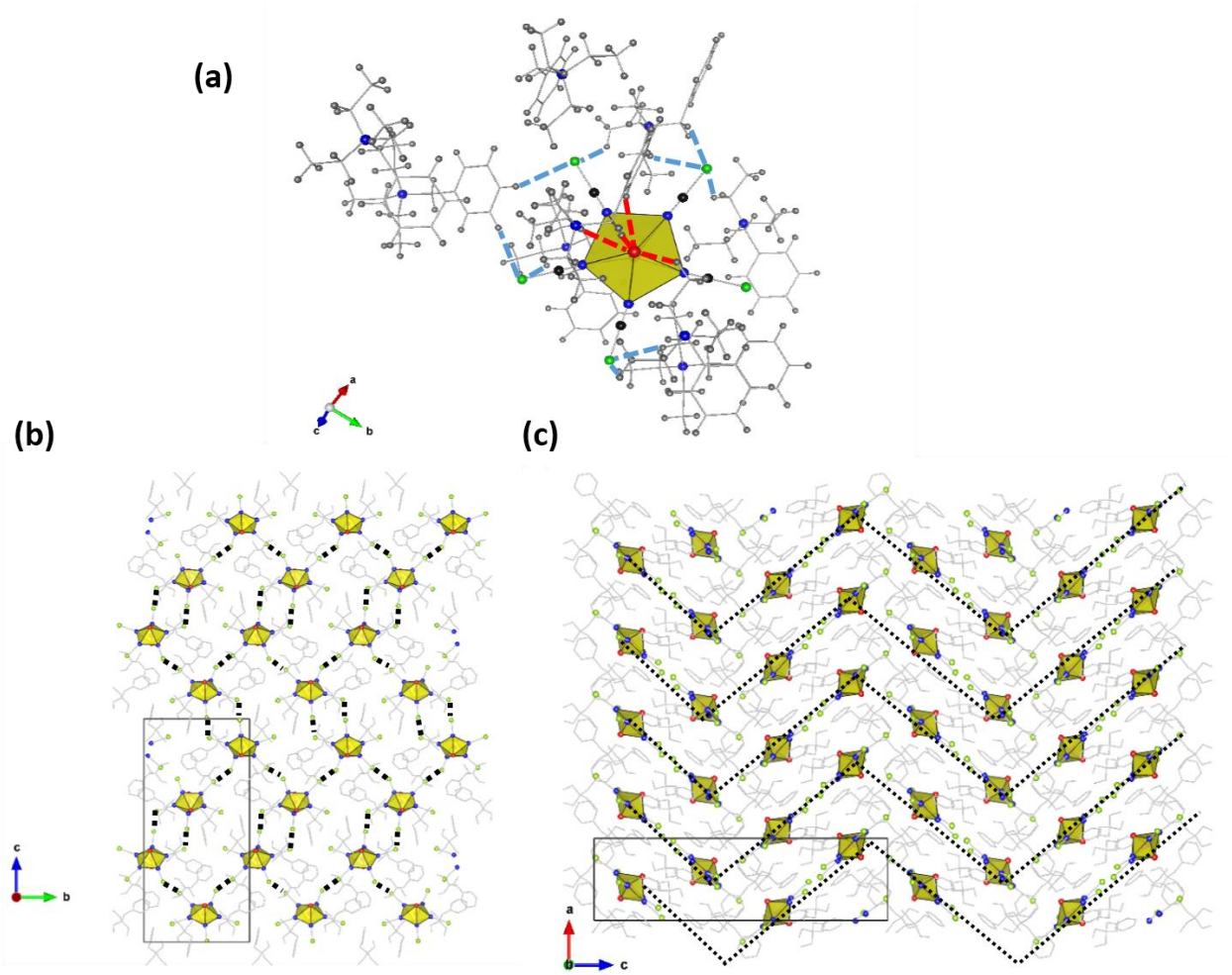

Figure 8. Supramolecular interactions in Et_3NBzSe: (a) a view of the C—H…O and C—H…Se; (b) the packing along the crystallographic *a*-axis and (c) along the crystallographic *b*-axis highlighting the chalcogenide interactions (dashed black line Se···Se; dashed red line U=O···H—C and dashed blue line Se···H—C).

(iii) Structural comparisons within the RS and RSe series – ^{n}PrS/^{n}PrSe and Et_3NBzS/Et_3NBzSe.

A summary of the types of interactions is shown in Table 3. We can directly compare structural parameters between two series with the same cation. For ^{n}Pr, the obvious conclusion is that the

chalcogenide···chalcogenide interactions are not present. Perhaps this is due to the non-rigid nature of the propyl arms which preferentially engage in S(e)···H—C and U=O···H—C interactions, implying that these are more favored over S(e)···S(e) interactions. The charge assisted hydrogen bonds to the uranyl ion are about the same length. Interestingly, the Et_3NBz series shows that as the polarizability of the chalcogenide atom increases then Type II interactions become preferred, even though these are isostructural pairs. The charge assisted hydrogen bond distances do not significantly change, indicating that perhaps these weak interactions are purely electrostatic in origin. A similar trend is observed for the S(e)···H—C interactions.

Table 3. Structural comparison of $[UO_2(NCE)_5]^{3-}$ compounds.

Compound	S···S (% vdv)	S···H—C	O···H—C	Compound	Se···Se	Se···H—C	O···H—C
MeS	Type I (95)	multiple	multiple	MeSe	Type I (101) Type II (100)	multiple	multiple
EtS	Type II (92)	multiple	multiple	EtSe	Type II (94)	multiple	multiple

^{n}PrS	no	multiple	multiple	^{n}PrSe	no	multiple	multiple
^{n}BuS	no	one	no	-			
Me_3BzNS	Type I (88)	multiple	multiple	-			
Et_3BzNS	Type I (94)	multiple	multiple	Et_3BzNSe	Type II (98)	multiple	multiple

A useful method for comparing solid state structures is via the Hirschfeld surfaces.[39] We have employed this method to examine the non-covalent interactions present in the RS and RSe series, along with selected other homoleptic uranyl thiocyanate complexes.[28,40] A quantitative analysis is shown in Figure 9. The chalcogenide···chalcogenide interactions decrease as the R group increases in size, but those with the R_3NBz group are type I for S and type II for Se. However it is clear that the S(e)···H—C interactions are the largest non-covalent interaction present but also decrease in the same order.

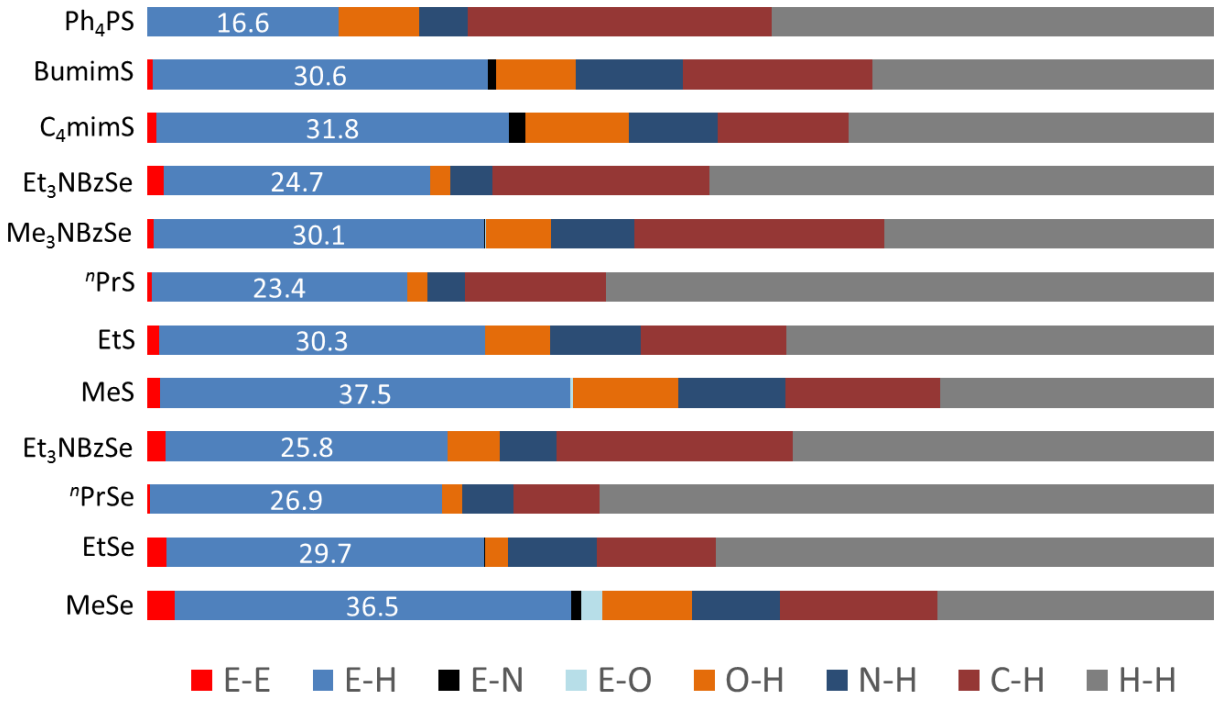

Figure 9. Quantitative Hirschfield analysis of RS and RSe series. (BumimS and C_4mimS from references 28 and 40 respectively)

Spectroscopic characterization.

All the compounds discussed above have been characterized spectroscopically with the aim of observing if the structural perturbations are detectable. NMR spectroscopy is uninformative, while solid-state ^{77}Se NMR spectroscopy does not show a clear trend (Figure S25).

Vibrational Spectroscopy. The vibrational spectra of crushed single crystals clearly show the uranyl stretch and the N=C and C=S(e) bond stretches. In the series the bands attributable to these stretches do not change significantly (Table S15); the Raman active ν_1(U=O) symmetric stretching mode lies in a narrow range between 842 and 850 cm^{-1} while the IR active ν_3(U=O) asymmetric

stretching mode comes between 910 and 940 cm^{-1} (Figures S7-S8). For comparison, the $[UO_2(H_2O)_5]^{2+}$ ion shows these bands at ca. 860-880 cm^{-1} and 930-960 cm^{-1} for the ν_1 and ν_3 modes respectively;[41] the presence of the donor atoms in the equatorial plane cause a redshift, as expected. From the IR and Raman spectra the stretching force constant (k_1) and the interaction force constant (k_{12}) can be calculated, as k_1 gives an indication of bond strength while k_{12} describes the interaction between the two –yl oxygen atoms.[42] In our case any changes must be due to the difference in the hydrogen bonding, and we can benchmark our data to the unperturbed U=O bond of ^{n}BuS. The force constants do not change significantly from this value (^{n}BuS, k_1 = 6.92 mdyn/Å; range = 6.84 – 7.06 mdyn/Å) and there is no correlation to the donor···acceptor bond distances (Table S15) so the hydrogen bonding does not influence these metrics, as observed by others.[22] There is however a larger k_1 and k_{12} associated with the NCSe ligands compared to the NCS analogues as shown for the ^{n}PrS/^{n}PrSe (S: k_1 = 6.91 mdyn/Å, k_{12} = -0.14 mdyn/Å; Se: k_1 = 6.98 mdyn/Å, k_{12} = -0.14 mdyn/Å) and Et_3NBzS/Et_3NBzSe (S: k_1 = 6.78 mdyn/Å, k_{12} = -0.10 mdyn/Å; Se: k_1 = 6.86 mdyn/Å, k_{12} = -0.17 mdyn/Å) families. The structural information showed no significant changes in donor···acceptor bond lengths, so this could be a manifestation of the differing donor abilities of the coordinating ligands.[20a]

Photoluminescence Spectroscopy. The photophysical properties of the uranyl ion have been well studied and the optical properties are due to a ligand-to-metal charge transfer (LMCT) transition involving promotion of an electron from bonding –yl oxygen orbitals (σ_u, σ_g, π_u and π_g) to non-bonding uranium $5f_\delta$ and $5f_\phi$ orbitals, centered at ca. 420 nm. The characteristic green emission at ca. 520 nm arises from de-excitation of the $^3\Pi_u$ triplet excited state. Superimposed on the absorption and emission bands are bands arising from strong coupling of the ground state Raman active symmetric vibrational O=U=O (ν_1) mode with the $^3\Pi_u$ electronic triplet excited state.[43]

There are some general trends that are apparent in the luminescence measurements, such as a correlation between the electron donating ability of the ligand and the $E_{0\text{-}0}$ values; i.e. the more electron donating the ligand the lower the energy value of the emission.[44] We recently showed for a series of $[UO_2X_4]^{2-}$ ions (X = Cl, Br, I) that the emission maxima and lifetimes of the $O_{yl}\rightarrow U$ LMCT band are not particularly sensitive to variation of the halide.[45] Recently the influence of the tecton in $[UO_2Cl_4]^{2-}$ has been interrogated using luminescence spectroscopy[46] and it may be that those ligands that have vibrational modes that can couple with the U=O vibrations to directly influence the luminescence properties. The emission and excitation spectra of RS and RSe have been recorded both in the solid state and in solution, where all non-covalent interactions break up and mononuclear species dominate.[47] In the solution emission spectra (Figure S22 and Table S16) there are clear differences between the RS and RSe family and the $[NCS]^-$ ion is a more electron donating ligand than the $[NCSe]^-$ ion in this series and on par with the nitrate ion. The differences within each family are small and mainly due to the changes in the vibronic coupling, and is also observed in the room temperature solid state emission spectra (Figure S23). Given the poor resolution of these spectra, we investigated the low temperature (77 K) photoluminescent properties of all compounds and selected examples are shown in Figure 10 (Figure S24 shows the remainder, except for MeSe which did not show any resolution enhancement). Immediately apparent is the increase in resolution, to the point that additional weaker bands appear, and are labelled as set A and B. The weak bands of set B are separated from each other by a vibrational progression of ca. 850 cm^{-1} which is due to coupling to the ν_1(U=O) vibration, but the differences between set A and B are ca 490 cm^{-1}. It is noteworthy that these additional bands were observed in the room temperature emission spectra of $[UO_2(NCS)_5]^{3-}$ in ionic liquids and ascribed to changes in the coordination environment. However a close examination of the Raman spectra of the RS

compounds show a number of rather weak bands at 500 and 544 cm^{-1} due to the δ(NCS) mode,[48] so it appears that this can couple with the uranyl vibrational mode; the same pattern is observed in $[Ph_4P]_2[UO_2(NCS)_3(NO_3)]$ (Figure S24). Supporting this is the smaller and weaker coupling of ca. 450 cm^{-1} in the RSe family which corresponds to the very weak δ(NCSe) vibrational bend at ca. 430 cm^{-1} in the Raman spectra (Figues S9). The only other mode that could couple is the U—N bend but in An(IV) thiocyanates this comes at ca 200 cm^{-1}.[49] The differences between the RS and RSe families are not marked at low temperature. Finally we have measured the lifetimes of the emissions both in the solid state and solution (Table S16), and they vary substantially across the series so no definitive conclusions can be drawn.

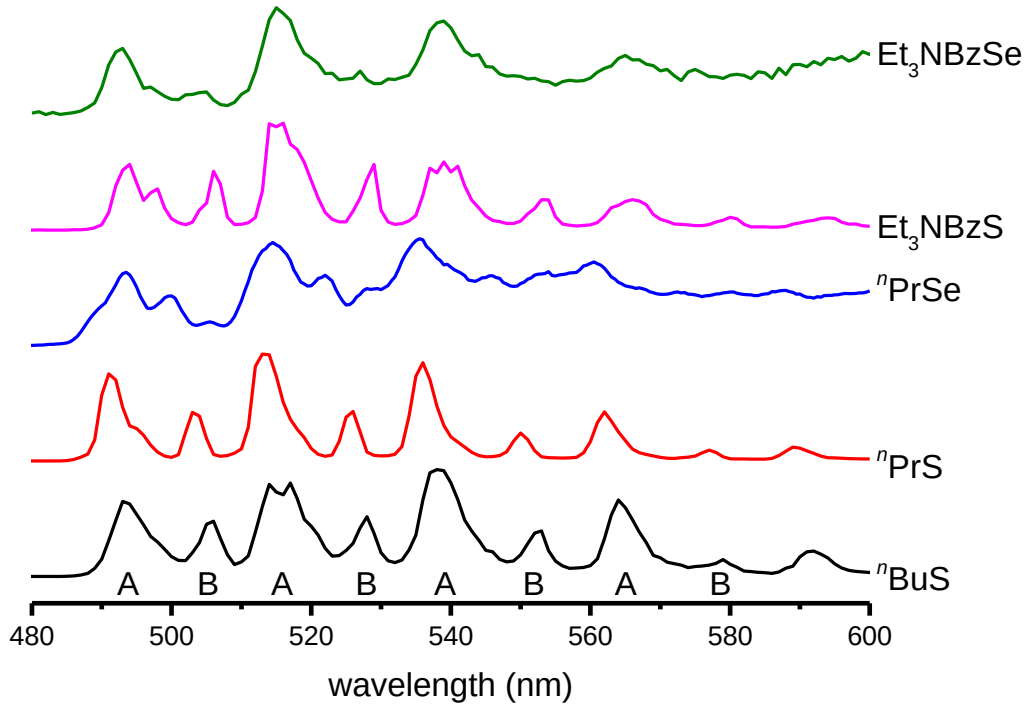

Figure 10. Emission spectra of selected examples of RS and RSe at 77 K in the solid state (λ_{ex} = 340 nm).

In summary, the spectroscopic data show some small differences between the [NCS] and [NCSe] coordinated ions, but suggest that the C—H···O interactions are not sufficiently strong to perturb the electronic structure of the uranyl ion, while the consequences for chalcogenide interactions are not observable.

DFT calculations.

To deepen our understanding of the non-covalent interactions in these species, we turned to DFT calculations. Supramolecular calculations of energy would be dominated by charge-charge interactions, so instead we have used molecular electrostatic potential (MEP), Atoms-in-Molecules (AIM) and natural bond orbital (NBO) derived properties to characterize U=O···H—C, Se···H—C and chalcogenide interactions in molecules and dimers selected from the crystal structures reported herein.

(i) Chalcogenide interactions. Se···Se interactions in $[Et_4N]_4[UO_2(NCSe)_5][NCSe]$, where the Se···Se distances are substantially shorter than the van der Waals radii, lead us to hypothesize the presence of a σ-hole on Se. Figure 11 shows the molecular electrostatic potential projected onto the 0.001 au isodensity surface for $[UO_2(NCS)_5]^{3-}$ and $[UO_2(NCSe)_5]^{3-}$. The overall negative charge of each complex means that the MEP is negative across the entire surface, but the plots nevertheless show regions of relative electron depletion (*i.e.* a σ-hole) on both S and Se, with a more pronounced hole on Se (-0.231 au) than on S (-0.246 au). There are also small differences in the –yl oxygens and corroborates the differing electron donating ability of the ligands from the photoluminescence spectroscopy and force constants.

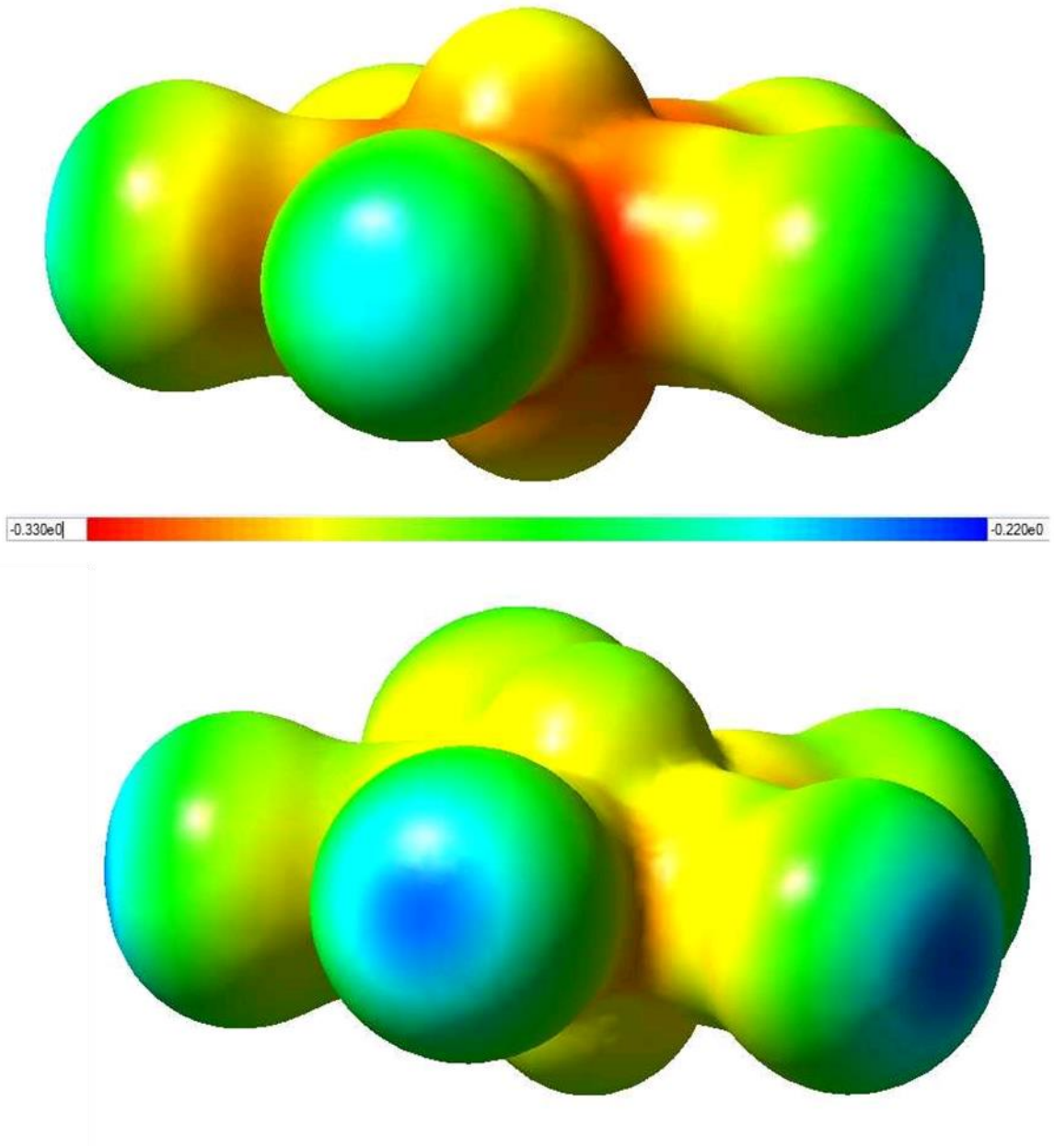

Figure 11. Molecular electrostatic potential projected onto the 0.001 au isodensity surface for $[UO_2(NCS)_5]^{3-}$ (top) and $[UO_2(NCSe)_5]^{3-}$ (bottom).

We elected to do DFT calculations for dimers of $[UO_2(NCSe)_5]^{3-}$ from MeSe and the complex of $[UO_2(NCSe)_5]^{3-}$ with $NCSe^-$ extracted from EtSe, as these gave representative examples of the weak interactions present in the series. NBO analysis indicates that the major interactions between species are donation from a Se lone pair of the coordinated $[NCSe]^-$ to a σ* orbital on another $[NCSe]^-$ moiety (1.94 kcal/mol and 0.58 kcal/mol) in the dimers extracted from MeSe. In the dimer extracted from EtSe, donation from a Se lone pair of the coordinated $[NCSe]^-$ to the C=Se σ* orbital of free $[NCSe]^-$ (2.94 kcal/mol), along with donation from the free Se lone pair to the coordinated C=Se σ* orbital (2.20 kcal/mol). Figure 12 shows the orbitals involved in EtSe. The energies of the MeSe dimers are lower than that of EtS and in keeping with the longer Se…Se distances in the structures. Finally, the interaction energies of model compounds $Me_2Se\cdots SeMe_2$ (-2.82 kcal/mol) and $Me_2Se\cdots Se(Me)CN$ (-4.62 kcal/mol)[50] are comparable to our systems.

The value of the electron density at the critical point, ρ_{bcp}, is often taken as a proxy for bond strength. Here the Se···Se contact exhibits a bond critical point with $\rho_{bcp} = 0.009$ au for both dimers, corroborating the NBO analysis that a weak but a stabilizing interaction is present. This is noteworthy as in MeSe the Se…Se contacts were slightly greater than the sum of the van der Waals radii. There are few reports of Se…E examples characterized via this methodology to compare, but $XRSe\cdots OH_2$ and $XRSe\cdots NH_3$ (R = H; Me; X = H, F, Me, CF_3, Cl, OH, OMe, NH_2, NHMe, CN) ρ_{bcp} range from 0.053-0.270 au for the Se···O/N interaction, or in $F_2C{=}Se\cdots NX$ (X = CH; H_3; HCH_2; CLi; Me_3; $\rho_{bcp} = 0.0089$-0.0197) and $F_2C{=}Se\cdots XY$ (XY = BrCl, ClF and BrF; $\rho_{bcp} = 0.0276$-0.0440).[51] The optimized dimers of $(X_2C{=}S)_2$ range from $\rho_{bcp} = 0.039$ to 0.050 with the sum of the charge transfer 1.52 to 3.12 kcal/mol (X = H, NH_2, OH, F, Cl).[11] This data can be put into a broader context by comparing to other non-conventional bonding that has been reported. Whilst it is clear that substitution effects are important, these chalcogenide interactions are on par with the

weak fluorine bonding (e.g. ρ_{bcp} = 0.0073 for the interaction in H—F…F—F[52]), or halogen lone pair…π interactions,[53] and weaker than, for example, F—Br..I—F (ρ_{bcp} = 0.0320)[54] as anticipated from the σ-hole mechanism of bonding which depends on the polarizability of the atom.

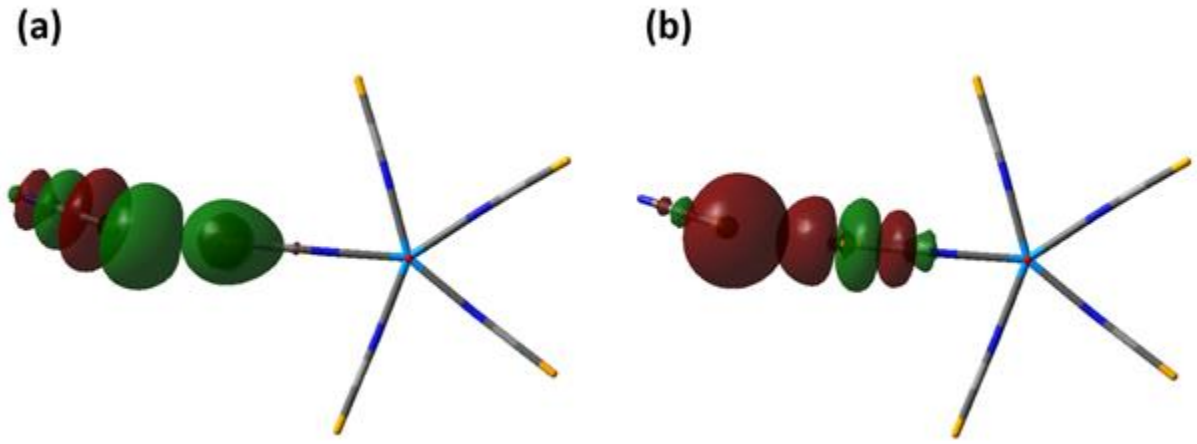

Figure 12. Theoretical analysis of $[Et_4N]_4[UO_2(NCSe)_5][NCSe]$ (a) NBO orbitals involved in the coordinated to free, (b) free to bound lone pair to σ* orbitals.

(ii) weak hydrogen bonding. We have characterized dimers bound by Se···H—C and U=O···H—C hydrogen bonding, taken from MeSe and ^{n}PrSe, an AIM approach as this features interactions. A dimer taken from MeSe contains three C—H···O=U bond critical points with ρ_{bcp} = 0.007, 0.006 & 0.005, while the H-bonds from ^{n}PrSe: 6 x C—H···Se = 0.008, 0.006, 0.005, 0.005, 0.004, 0.003. Thus, individual C—H···Se are individually weak but rather numerous, lending support to the hypothesis that these dominate in cases such as ^{n}PrSe with many such donors. C—H···O=U interactions seem even weaker on this basis, again supporting the observation noted above that the terminal O in uranyl are relatively weak Lewis bases. *Intra*molecular C—H···O=U hydrogen

bonding has recently been theoretically analyzed and in this case ρ_{bcp} = 0.002-0.0243 a.u., indicating that intramolecular hydrogen bonding is perhaps stronger than intermolecular hydrogen bonding, although geometric constraints may influence this.

Conclusions

A series of uranyl thiocyanate and selenocyanate compounds have been prepared and structurally characterized. The nature of the alkyl ammonium group dictates the non-covalent interactions observed in the solid state and chalcogenide, C—H···O=U and C—H···S(e) are observed. Chalcogenide interactions are observed in some of the structures and are more prevalent in the [NCSe] series than the [NCS], and in line with the increased polarizability of the Se which renders a more pronounced σ-hole on Se (-0.231 au from MESP) than on S (-0.246 au from MESP). The molecular orbitals responsible for this were identified and correspond with the known ideas of n to σ* charge transfer in these non-classical interactions, albeit in this example the non-bonded pair of electrons resides in a σ orbital. Comparison with other weak σ-hole type bonds puts these chalcogenide interactions similar to interactions involving fluorine or, more commonly used in synthetic chemistry, lone pair···π interactions.[55] C—H···S(e) interactions are individually weak from an AIM analysis but numerous and accounts for their preponderance in the solid state structures. The vibrational data suggest that the charge assisted hydrogen bonding to the –yl oxygens does not influence the spectroscopic properties and DFT studies show that these interactions are the weakest of the three studied. Unusually, the coupling the δ(NCS) and δ(NCSe) vibrational modes to the uranyl mode manifests itself in the photophysical properties of these species in the solid state. Taken together these results show that collectively non-classical

interactions can have an important influence of the solid state structures, but are in these cases not observable by conventional spectroscopic techniques. Nonetheless, these add to the growing field of chalcogenide interactions in the coordination sphere of metals.

Experimental Section

Caution! Natural uranium was used during the course of the experimental work. As well as the radiological hazards, uranium is a toxic metal and care should be taken with all manipulations. Experiments using uranium materials were carried out using pre–set radiological safety precautions in accordance with the local rules of Trinity College Dublin.

^{1}H, $^{13}C\{^{1}H\}$, $^{31}P\{^{1}H\}$ and $^{77}Se\{^{1}H\}$ spectra were recorded on a Bruker AV400 spectrometer operating at 400.23 MHz, 155.54 MHz, 161.98 MHz and 76.33 MHz respectively, and were referenced to the residual ^{1}H and ^{13}C resonances of the solvent used or external H_3PO_4 or Me_2Se. Solid state ^{77}Se NMR spectra were recorded on a Bruker 400 HD at 76.3 MHz.IR spectra were recorded on a Perkin Elmer Spectrum One spectrometer with attenuated total reflectance (ATR) accessory. Raman spectra were obtained using 785-nm excitation on a Renishaw 1000 micro-Raman system. UV-vis measurements were made on a Perkin Elmer Lambda 1050 spectrophotometer, using fused silica cells with a path length of 1 cm. Steady-state photoluminescence spectra were recorded on a Horiba-Jobin-Yvon Fluorolog-3 spectrofluorimeter. Luminescence lifetime data were recorded following 372-nm excitation, using time-correlated single-photon counting (a PCS900 plug-in PC card for fast photon counting). Lifetimes were obtained by tail fit on the data obtained, and the quality of fit was judged by

minimization of reduced chi-squared and residuals squared. X-ray crystallography data were measured on a Bruker Apex diffractometer at 100 K. The structure was solved by direct methods and refined by least squares method on F^2 using the SHELXTL program package.[56] Crystal data, details of data collections and refinement are given in Table S17. CCDC 1586895-1586903 contains the supplementary crystallographic data for this paper. This data can be obtained free of charge from The Cambridge Crystallographic Data Centre via www.ccdc.cam.ac.uk/data_request/cif. Structural figures were prepared using VESTA[57] or mercury. All other chemicals and solvents were obtained from commercial sources and used as received.

DFT calculations were carried out using the meta-hybrid M06-2X[58] DFT method Gaussian09,[59] without symmetry constraints. Monomer or dimer coordinates were extracted from relevant crystal structures, and where necessary C—H bond lengths normalized to values from neutron diffraction (1.082 Å), with all heavy atom positions frozen at crystalline values. Scalar relativistic effects in uranium were included through use of effective core potentials as defined in Preuss et al's ECP/basis set on U,[60] while for lighter atoms 6-31+G(d,p) was used. Natural bond orbital (NBO) analysis was performed using Gaussian09; Atoms-in-Molecules (AIM) analysis used AIMAll.[61] Topological analysis of the electronic density (ρ) is based upon those points where the gradient of the density, $\nabla\rho$, vanishes. In this work we consider points where one curvature (in the inter-nuclear direction) is positive and two (perpendicular to the bond direction) are negative, termed (3, -1) or bond critical points. Properties evaluated at such points characterize the bonding interactions present.

All solvents and reagents were obtained commercially and used as received. $[R_4N]_3[UO_2(NCS)_5]$ (R = Me, Et, ^{n}Pr) were synthesized via a slight modification of literature procedure, whereby the reactants were mixed in MeCN rather than H_2O.

Synthesis of uranyl thiocyanates

To a solution of $UO_2(NO_3)_2 \cdot 6H_2O$ (0.30 g) in acetonitrile (30 cm^3) were added Na[NCS] (5 equivalents) and the appropriate cation (3 equivalents). The solution mixture was stirred at room temperature for 60 minutes. The resulting yellow solution was filtered and the solvent was reduced in volume. Crystals suitable for X-ray diffraction were obtained by vapor diffusion of ^{i}Pr$_2$O into MeCN solutions of the products and yellow crystals obtained after ca. 1 week.

$[^n Bu_4N]_3[UO_2(NCS)_5]$. Yield: 57%, 0.44 g; ^{1}H NMR (400 MHz, CD_3CN): δ 1.00 ppm (t, 36H, J_{H-H} = 7.36 Hz, CH_3), δ 1.38 ppm (m, 24H, J_{H-H} = 7.43 Hz, CH_2), δ 1.63 ppm (m, 24H, J_{H-H} = 8.55 Hz, CH_2), δ 3.11 ppm (m, 24H, J_{H-H} = 8.62 Hz, CH_2); $^{13}C\{^1H\}$ NMR (155 MHz, CD_3CN): δ 12.89 ppm (CH_3), δ 19.39 ppm (CH_2), δ 23.36 ppm (CH_2), δ 58.33 ppm (CH_2); IR (ATR, ν/cm^{-1}): 2960 (m), 2872 (w), 2052 (s, C=N), 1467 (m), 1380 (w), 1152 (w), 1108 (w), 1067 (w), 1026 (w), 919 (s, U=O), 882 (m), 736 (m, C=S); Raman (ν/cm^{-1}): 2099 and 2059 (C=N), 1456, 1324, 909, 850 (U=O), 736 (C=S); UV-vis (ε, dm^3 mol^{-1} cm^{-1}): (298 K, MeCN, ~10^{-5} M): 330 nm (4868), 284 nm (6240.5), 232 nm (17618).

$[Me_3NBz]_3[UO_2(NCS)_5]$. Yield: 55%, 0.29 g; ^{1}H NMR (400 MHz, CD_3CN): δ 3.05 ppm (s, 27H, CH_3), δ 4.43 ppm (s, 6H, CH_2), δ 7.52 ppm (m, 6H, o-CH), δ 7.53 ppm (m, 3H, p-CH), δ 7.56 ppm (m, 6H, m-CH); $^{13}C\{^1H\}$ NMR (155 MHz, CD_3CN): δ 52.4 ppm (CH_3), δ 69.3 ppm (CH_2), δ 127.6

ppm (ipso-C), δ 129.2 ppm (m-CH), δ 130.7 ppm (p-CH), δ 132.9 ppm (o-CH); IR (ATR, ν/cm^{-1}): 3420 (m), 3025 (w), 2030 (s, C=N), 1634 (w), 1581 (w), 1475 (m), 1408 (m), 1375 (m), 1211 (m), 1076 (w), 1036 (w), 970 (m), 916 (s, U=O), 885 (m), 779 (m, C=S), 725 (s), 700 (s); Raman (ν/cm^{-1}): 2090 and 2062 and 2048 and 2041 (C=N), 1065, 1584, 1471, 1446, 1216, 1184, 1157, 1033, 1003, 845 (U=O), 823, 808 (C=S), 725, 621; UV-vis (ε, dm^3 mol^{-1} cm^{-1}), (298 K, MeCN, ~10^{-5} M): 342 nm (14461), 300 nm (17597).

$[Et_3NBz]_3[UO_2(NCS)_5]$. Yield: 62%, 0.41 g; ^{1}H NMR (400 MHz, CD_3CN): δ 1.37 ppm (t, 27H, J_{H-H} = 7.11 Hz, CH_3), δ 3.18 ppm (q, 18H, J_{H-H} = 7.18 Hz, CH_2), δ 4.35 ppm (s, 6H, CH_2), δ 7.51 ppm (m, 3H, p-CH), δ 7.53 ppm (m, 6H, m-CH), δ 7.55 ppm (m, 6H, o-CH); ^{13}C{^{1}H} NMR (155 MHz, CD_3CN): δ 8.13 ppm (CH_3), δ 53.5 ppm (CH_2), δ 61.1 ppm (CH_2), δ 128.1 ppm (ipso-C), δ 130.2 ppm (m-CH), δ 131.5 ppm (p-CH), δ 133.4 ppm (o-CH); IR (ATR, ν/cm^{-1}): 3437 (w), 2994 (w), 2086 (m), 2042 (s, C=N), 1455 (m), 1399 (m), 1330 (w), 1214 (w), 1182 (w), 1150 (m), 1086 (m), 1033 (m), 1005 (m), 910 (s, U=O), 788 (m) 752 (s, C=S), 693 (s); Raman (ν/cm^{-1}): 2089 and 2042 (C=N), 1005, 842 (U=O), 816 and 812 and 804 (C=S), 679; UV-vis (ε, dm^3 mol^{-1} cm^{-1}), (298 K, MeCN, ~10^{-5} M): 333 nm (4268) nm, 286 nm (5610), 230 nm (8503).

$[Ph_4P]_2[UO_2(NCS)_3(NO_3)]$. Yield: 51%, 0.36 g; ^{1}H NMR (400 MHz, CD_3CN): δ 7.71 ppm (m, 8H, J_{H-H} = 8.43 Hz, m-CH), δ 7.78 ppm (m, 8H, J_{H-H} = 7.93 Hz, o-CH), δ 7.95 ppm (m, 4H, J_{H-H} = 7.53 Hz, p-CH); ^{13}C{^{1}H} NMR (155 MHz, CD_3CN): δ 118.4 ppm (d, $^1J_{P-C}$ = 89.60 Hz ipso-C), δ 130.3 ppm (d, $^3J_{P-C}$ = 12.8 Hz, m-CH), δ 134.7 ppm (d, $^2J_{P-C}$ = 10.3 Hz, o-CH), δ 135.4 ppm (d, $^4J_{P-C}$ = 2.94 Hz, p-CH); ^{31}P{^{1}H} NMR (162 MHz, CD_3CN): δ 22.7 ppm; IR (ATR, ν/cm^{-1}): 3054 (w), 2029 (s, N=C), 1584 (w), 1481 (w), 1433 (m), 1341 (w), 1312 (w), 1269 (w), 1189 (w), 1163

(w), 1104 (s), 1025 (w), 996 (m), 928 (s, U=O), 754 (m, C=S), 720 (s), 678 (s), 616 (w), 523 (s); Raman (ν/cm^{-1}): 2079 and 2034 (C=N), 1586, 1575, 1187, 1165, 1111, 1095, 1037, 1001, 860 (U=O), 826 and 819 (C=S), 677, 615, 278, 257, 244; UV-vis (ε, dm^3 mol^{-1} cm^{-1}), (298 K, MeCN, ~10^{-5} M): 330 nm (4727), 275 nm (11131), 232 (49865).

Synthesis of uranyl selenocyanates

To a solution of $UO_2(NO_3)_2 \cdot 6H_2O$ (0.30 g) in acetonitrile (30 cm^3) were added KNCSe (5 equivalents) and the appropriate cation (3 equivalents). The solution mixture was stirred at room temperature for 60 minutes in the dark. The resulting orange solution was filtered and the solvent was reduced in volume. Crystals suitable for X-ray diffraction were obtained by vapor diffusion of $^{i}Pr_2O$ into MeCN solutions of the products and yellow crystals obtained after ca. 1 week.

$[Me_4N]_3[UO_2(NCSe)_5].H_2O$. Yield: 39%, 0.20 g; ^{1}H NMR (400 MHz, CD_3CN): δ 3.14 ppm (s, 12H, CH_3), δ 2.25 ppm (s, 2H, H_2O); $^{13}C\{^1H\}$ NMR (155 MHz, CD_3CN): δ 54.9 ppm (CH_3); $^{77}Se\{^1H\}$ NMR (76 MHz, CD_3CN): δ -340.5 ppm (NCSe); IR (ATR, ν/cm^{-1}): 3027 (w), 2956 (w), 2060 and 2042 (s, C=N), 1738 (w), 1480(m), 1410 (w), 1365 (w), 944 (s), 920 (s, U=O), 632 (m, C=Se); Raman (ν/cm^{-1}): 2071 and 2091 (C=N), 1460, 948, 848 (U=O), 753 (C=Se), 637, 564, 457, 250; UV-vis (ε, dm^3 mol^{-1} cm^{-1}), (298 k, MeCN, ~10^{-5} M): 329 nm (7311), 250 nm (25068).

$[^{n}Pr_4N]_3[UO_2(NCSe)_5]$. Yield: 45%, 0.36 g; ^{1}H NMR (400 MHz, CD_3CN): δ 0.977 ppm (t, 36H, J_{H-H} = 7.27 Hz, CH_3), δ 1.69 ppm (m, 18H, J_{H-H} = 9.27 Hz, CH_2) δ 3.10 ppm (m, 18H, J_{H-H} = 5.20 Hz, CH_2); $^{13}C\{^1H\}$ NMR (155 MHz, CD_3CN): δ 10.8 ppm (CH_3), δ 16.0 ppm (CH_2), δ 61.0 ppm

(CH_2); $^{77}Se\{^1H\}$ NMR (76 MHz, D-Acetone): δ -305 ppm (NCSe); IR (ATR, ν/cm^{-1}): 2968 (m), 2937 (w), 2877 (w), 2094 (w), 2060 and 2046 (s, C=N), 1482 (m), 1455 (m), 1385 (m), 968 (m), 926 (s, U=O), 842 (w), 756 (m, C=Se), 627 (m); Raman (ν/cm^{-1}): 2100 and 2079 and 2065 (C=N), 1459, 1316, 1140, 1110, 1037, 852 (U=O), 783, 757, 640 (C=Se), 557, 333, 313, 210; UV-vis (ε, dm^3 mol^{-1} cm^{-1}), (298 k, MeCN, ~10^{-5} M): 330 nm (9696).

$[Et_3NBz]_3[UO_2(NCSe)_5]$. Yield: 54%, 0.44 g; ^1H NMR (400 MHz, D-Acetone): δ 1.55 ppm (t, 27H, J_{H-H} = 7.31 Hz, CH_3), δ 3.47 ppm (q, 18H, J_{H-H} = 7.33 Hz, CH_2), δ 4.70 ppm (s, 6H, CH_2), δ 7.55 ppm (m, 3H, p-CH), δ 7.57 ppm (m, 6H, m-CH), δ 7.66 ppm (m, 6H, o-CH); $^{13}C\{^1H\}$ NMR (155 MHz, D-Acetone): δ 7.35 ppm (CH_3), δ 52.7 ppm (CH_2), δ 60.3 ppm (CH_2), δ 128 ppm (ipso-C), δ 129 ppm (m-CH), δ 131 ppm (p-CH), δ 133 ppm (o-CH); $^{77}Se\{^1H\}$ NMR (76 MHz, D-Acetone): δ -342 ppm (NCSe); IR (ATR, ν/cm^{-1}): 2984 (w), 2086 (w), 2047 (s, C=N), 1451 (m), 1395 (m) 1210 (w), 1186 (w), 1154 (m), 1078 (w), 1030 (m), 969 (w), 920 (s, U=O), 831 (w), 806 (w), 791 (m), 751 (s, C=Se), 701 (s); Raman (ν/cm^{-1}): 2087 and 2056 and 2043 (C=N), 1604, 1460, 1212, 1051, 1033, 1003, 842 (U=O), 677, 643, 624; UV-vis (ε, dm^3 mol^{-1} cm^{-1}), (298 k, MeCN, ~10^{-5} M): 329 nm (5383), 264 nm (8167), 248 nm (18259).

ASSOCIATED CONTENT

AUTHOR INFORMATION

Corresponding Author

* Tel: +353-1-8963501. Fax: +353-1-6712826. E-mail: bakerrj@tcd.ie

Author Contributions

The manuscript was written through contributions of all authors. All authors have given approval to the final version of the manuscript.

ACKNOWLEDGMENT

We thank TCD for funding this work.

Supporting Information. Full crystallographic descriptions (CIF), spectroscopic and computational details. This material is available free of charge via the Internet at http://pubs.acs.org.

REFERENCES

(1) For recent reviews see: (a) Cavallo, G.; Metrangolo, P.; Milani, R.; Pilati, T.; Priimagi, A.; Resnati, G.; Terraneo G. The Halogen Bond. *Chem. Rev.* **2016**, 116, 2478–2601; (b) Gilday, L. C.; Robinson, S. W.; Barendt, T. A.; Langton, M. J.; Mullaney, B. R.; Beer, P. D. Halogen Bonding in Supramolecular Chemistry. *Chem. Rev*. **2015**, 115, 7118-7195; (c) Bishop, R. Organic crystal engineering beyond the Pauling hydrogen bond. *CrystEngComm*. **2015**, 17, 7448-7460; (d) Troff, R. W.; Makela, T. Topic, F.; Valkonen, A.; Raatikainen, K.; Rissanen, K. Alternative Motifs for Halogen Bonding. *Eur. J. Org. Chem.* **2013**, 1617-1637.

(2) (a) Del Bene, J. E.; Alkorta, I.; Elguero, J. *Noncovalent Forces: Challenges and Advances in Computational Chemistry and Physics*, ed. Scheiner, S. Springer: New York, **2015**, *19*, 191–263; (b) Setiawan, D.; Kraka, E.; Cremer, D. Strength of the Pnicogen Bond in Complexes Involving Group Va Elements N, P, and As. *J. Phys. Chem. A* **2015**, 119, 1642–1656; (c) Sarkar, S.; Pavan, M. S.; Guru Row, T. N. Experimental validation of 'pnicogen bonding' in nitrogen by charge

density analysis. *Phys. Chem. Chem. Phys.* **2015**, 17, 2330–2334; (d) Guan, L.; Mo, Y. Electron Transfer in Pnicogen Bonds. *J. Phys. Chem. A* **2014**, *118*, 8911–8921; (e) Del Bene, J. E.; Alkorta, I.; Elguero, J. Pnicogen-Bonded Anionic Complexes. *J. Phys. Chem. A* **2014**, 118, 3386–3392; (f) Politzer, P.; Murray, J. S.; Janjić, G. V.; Zarić, S. D. σ-Hole Interactions of Covalently-Bonded Nitrogen, Phosphorus and Arsenic: A Survey of Crystal Structures. *Crystals* **2014**, *4*, 12–31; (g) Scheiner, S. The Pnicogen Bond: Its Relation to Hydrogen, Halogen, and Other Noncovalent Bonds. *Acc. Chem. Res.* **2013**, *46*, 280–288; (h) Scheiner, S. Detailed comparison of the pnicogen bond with chalcogen, halogen, and hydrogen bonds. *Int. J. Quantum Chem.* **2013**, *113*, 1609–1620; (i) Eskandri, K.; Mahmoodabadi, N. Pnicogen Bonds: A Theoretical Study Based on the Laplacian of Electron Density. *J. Phys. Chem. A* **2013**, 117, 13018–13024; (j) Adhikary, U.; Scheiner, S. *J. Chem. Phys.* **2011**, *135*, 184306; (k) Zahn, S.; Frank, R.; Hey-Hawkins, E.; Kirchner, B. Pnicogen Bonds: A New Molecular Linker? *Chem. – Eur. J.* **2011**, 17, 6034–6038; (l) Kilian, P.; Slawin, A. M. Z.; Woollins, J. D. Naphthalene-1,8-diyl Bis(Halogenophosphanes): Novel Syntheses and Structures of Useful Synthetic Building Blocks. *Chem. – Eur. J.* **2003**, 9, 215–222.

(3) Bauzá, A.; Frontera, A. Aerogen Bonding Interaction: A New Supramolecular Force? *Angew. Chem. Int. Ed.* **2015,** 54, 7340-7343.

(4) (a) Gleiter, R.; Haberhauer, G.; Werz, D. B.; Rominger, F.; Bleiholder, C. From Noncovalent Chalcogenide-Chalcogenide Interactions to Supramolecular Aggregates: Experiments and Calculations. *Chem. Rev.* **2018**, DOI:10.1021/acs.chem.rev.7b00449; (b) Pascoe, D. J.; Ling, K. B.; Cockroft S. L. The Origin of Chalcogen-Bonding Interactions. *J. Am. Chem. Soc.* **2017**, 139, 15160-15167; (b) Huynh, H. –T.; Jeannin, O.; Fourmigué, M. Organic selenocyanates as strong and directional chalcogen bond donors for crystal engineering. *Chem. Commun*. **2017**, 53, 8467-8469; (c) Oliveira, V.; Cremer, D.; Kraka, E. The Many Facets of Chalcogen Bonding: Described

by Vibrational Spectroscopy. J. Phys. Chem. A 2017, 121, 6845-6862; (d) Shukla, R.; Chopra, D. "Pnicogen bonds" or "chalcogen bonds": exploiting the effect of substitution on the formation of P···Se noncovalent bonds. *Phys. Chem. Chem. Phys.* **2016**, *18*, 13820-13829; (e) Pang, X.; Jin, W. J. Exploring the Halogen Bond Specific Solvent Effects in Halogenated Solvent Systems by Esr Probe. *New J. Chem.* **2015**, 39, 5477−5483; (f) Azofra, L. M.; Alkorta, I.; Scheiner, S. Chalcogen Bonds in Complexes of SOXY (X, Y = F, Cl) with Nitrogen Bases. *J. Phys. Chem. A* **2015**, 119, 535−541; (g) Si, M. K.; Lo, R.; Ganguly, B. The Origin and Magnitude of Intramolecular Quasi-Cyclic S··O and S··S Interactions Revisited: A Computational Study. *Chem. Phys. Lett.* **2015**, 631−632, 6−11; (h) Esrafili, M.; Mohammadian-Sabet, F. Ab Initio Calculations of Cooperativity Effects on Chalcogen Bonding: Linear Clusters of $(OCS)_{2–8}$ and $(OCSe)_{2–8}$. *Struct. Chem*. **2015**, 26, 199−206; (i) Nziko, V. d. P. N.; Scheiner, S. Intramolecular S···O Chalcogen Bond as Stabilizing Factor in Geometry of Substituted Phenyl-SF_3 Molecules. *J. Org. Chem.* **2015**, 80, 2356−2363; (j) Garrett, G. E.; Gibson, G. L.; Straus, R. N.; Seferos, D. S.; Taylor, M. S. Chalcogen Bonding in Solution: Interactions of Benzotelluradiazoles with Anionic and Uncharged Lewis Bases. *J. Am. Chem. Soc.* **2015**, *137*, 4126–4133; (k) Thomas, S. P.; Satheeshkumar, K.; Mugesh, G.; Guru Row, T. N. Unusually Short Chalcogen Bonds Involving Organoselenium: Insights into the Se–N Bond Cleavage Mechanism of the Antioxidant Ebselen and Analogues. *Chem. – Eur. J.* **2015**, 21, 6793–6800; (l) Shukla, R.; Chopra, D. Exploring the Role of Substitution on the Formation of Se···O/N Noncovalent Bonds. *J. Phys. Chem. B* **2015**, 119, 14857–14870; (m) Adhikari, U.; Scheiner, S. Effects of Charge and Substituent on the S···N Chalcogen Bond. *J. Phys. Chem. A* **2014**, 118, 3183−3192; (n) Tsuzuki, S.; Sato, N. Origin of Attraction in Chalcogen–Nitrogen Interaction of 1,2,5-Chalcogenadiazole Dimers. *J. Phys. Chem. B* **2013**, 117, 6849–6855; (o) Wang, W.; Ji, B.; Zhang, Y. Chalcogen Bond: A Sister Noncovalent Bond to Halogen Bond.

J. Phys. Chem. A **2009**, *113*, 8132–8135; (p) Murray, J. S.; Lane, P.; Politzer, P. Simultaneous σ-hole and hydrogen bonding by sulfur- and selenium-containing heterocycles. *Int. J. Quantum Chem.* **2008**, 108, 2770–2781; (q) Rosenfield, R. E.; Parthasarathy, R.; Dunitz, J. D. Directional Preferences of Nonbonded Atomic Contacts with Divalent Sulfur. 1. Electrophiles and Nucleophiles. *J. Am. Chem. Soc.* **1977**, 99, 4860− 4862.

(5) (a) Grabowski, S. J.; Sokalski, W. A. Are various sigma-hole bonds steered by the same mechanisms? *ChemPhysChem* **2017**, 18, 1569–1577; (b) Oliveira, V.; Kraka, E. Systematic Coupled Cluster Study of Noncovalent Interactions Involving Halogens, Chalcogens, and Pnictogens. *J. Phys. Chem. A* **2017**, 121, 9544-9556; (c) Wang, H.; Wang, W.; Jin, W. J. σ-Hole Bond vs π-Hole Bond: A Comparison Based on Halogen Bond. *Chem. Rev.* **2016***,* 116*,* 5072–5104; (c) Kolář, M. H.; Hobza P. Computer Modeling of Halogen Bonds and Other σ-Hole Interactions. *Chem. Rev.* **2016,** 116, 5155–5187; (d) Politzer, P.; Murray, J. S.; Clark, T. Halogen bonding and other σ-hole interactions: a perspective. *Phys. Chem. Chem. Phys*. **2013**, 15, 11178-11189; (e) Politzer, P.; Murray, J. S. Halogen Bonding: An Interim Discussion. *ChemPhysChem* **2013**, *14*, 278-294; (f) Politzer, P.; Murray, J. S.; Clark, T. *Phys. Chem. Chem. Phys.* Halogen bonding: an electrostatically-driven highly directional noncovalent interaction. **2010**, 12, 7748-7757.

(6) Scheiner, S. Comparison of CH···O, SH···O, Chalcogen, and Tetrel Bonds Formed by Neutral and Cationic Sulfur-Containing Compounds. *J. Phys. Chem. A* **2015**, 119, 9189−9199.

(7) Bauzá, A.; Mooibroek, T. J.; Frontera, A. The Bright Future of Unconventional σ/π-Hole Interactions. *ChemPhysChem* **2015**, 16, 2496-2517.

(8) Goettel, J. T.; Chaudhary, P.; Hazendonk, P.; Mercier, H. P. A.; Gerken, M. $SF_4 \cdot N(C_2H_5)_3$: the first conclusively characterized SF_4 adduct with an organic base. *Chem. Commun.* **2012**, 48, 9120–9122.

(9) Nziko, V. de P. N.; Scheiner S. Chalcogen Bonding between Tetravalent SF_4 and Amines. *J. Phys. Chem. A* **2014**, 118, 10849-10856.

(10) (a) Mukherjee, A.; Desiraju, G. R. Halogen bonds in some dihalogenated phenols: applications to crystal engineering. *IUCrJ* **2014**, 1, 49-60; (b) Tothadi, S.; Joseph, S.; Desiraju, G. R. Synthon Modularity in Cocrystals of 4-Bromobenzamide with n-Alkanedicarboxylic Acids: Type I and Type II Halogen···Halogen Interactions. *Cryst. Growth Des.* **2013**, 13, 3242-3254.

(11) Shukla, R.; Chopra, D. Crystallographic and Theoretical Investigation on the Nature and Characteristics of Type I C═S···S═C Interactions *Cryst. Growth Des.* **2016**, 16, 6734-6742.

(12) (a) Peacock, H.; Luo, J.; Yamashita, T.; Luccarelli, J.; Thompson, S.; Hamilton, A. D. Non-covalent S···O interactions control conformation in a scaffold that disrupts islet amyloid polypeptide fibrillation. *Chem. Sci.* **2016**, 7, 6435-6439; (b) Brezgunova, M. E.; Lie-rig, J.; Aubert, E.; Dahaoui, S.; Fertey, P.; Lebègue, S.; Ángyán, J. G.; Fourmigué, M.; Espinosa, E. Chalcogen Bonding: Experimental and Theoretical Determinations from Electron Density Analysis. Geometrical Preferences Driven by Electrophilic–Nucleophilic Interactions. *Cryst. Growth Des*. **2013**, 13, 3283-3289; (c) Iwaoka, M.; Isozumi, N. Hypervalent Nonbonded Interactions of a Divalent Sulfur Atom. Implicationsin Protein Architecture and the Functions. *Molecules*, **2012**, 17, 7266-7283; (d) Meyer, E. A.; Castellano, R. K.; Diederich, F. Interactions with Aromatic Rings in Chemical and Biological Recognition. *Angew. Chem. Int. Ed.* **2003**, 42, 1210-1250; (d) Iwaoka, M.; Takemoto, S.; Tomoda, S. Statistical and Theoretical Investigations on the Directionality of

Nonbonded S···O Interactions. Implications for Molecular Design and Protein Engineering. *J. Am. Chem. Soc.* **2002**, 124, 10613-10620.

(13) (a) Mahmudova, K. T.; Kopylovich, M. N.; Guedes da Silva, M. F. C.; Pombeiro, A. J. L. Non-covalent interactions in the synthesis of coordination compounds: Recent advances. *Coord. Chem. Rev.* **2017**, 345, 54-72; (b) Tiekink, E. R.T. Supramolecular assembly based on "emerging" intermolecular interactions of particular interest to coordination chemists. *Chem. Rev.* **2017**, 345, 209-228.

(14) Ivanov, D. M.; Novikov, A. S.; Ananyev, I. V.; Kirina, Y. V.; Kukushkin, V. Y. Halogen bonding between metal centers and halocarbons. *Chem. Commun*. **2016**, 52, 5565-5568.

(15) Mei, L.; Wang, C.-Z.; Wang, L.; Zhao, Y-L.; Chai, Z-F.; Shi, W.-Q. Halogen Bonded Three-Dimensional Uranyl–Organic Compounds with Unprecedented Halogen–Halogen Interactions and Structure Diversity upon Variation of Halogen Substitution. *Cryst. Growth Des.* **2015**, 15, 1395-1406.

(16) Baker, R. J. New Reactivity of the Uranyl(VI) Ion. *Chem. Eur. J.* **2012**, 18, 16258–16271.

(17) (a) Liu, H.; Ghatak, T.; Eisen, M. S. Organoactinides in catalytic transformations: scope, mechanisms and Quo Vadis. *Chem. Commun*. **2017**, 53, 11278-11297; (b) Walshe, A.; Fang, J.; Maron, L.; Baker, R. J. A New Mechanism for the Ring Opening Polymerization of Lactones? Uranyl Aryloxides Induces Intermolecular Catalysis. *Inorg. Chem.* **2013**, 52, 9077-9086; (c) Fang, J.; Walshe, A.; Maron, L.; Baker, R. J. Ring Opening Polymerization of Epoxides Catalyzed by Uranyl complexes: An Experimental and Theoretical Study of the Reaction Mechanism. *Inorg. Chem.* **2012**, 51, 9132-9140; (d) Baker, R. J.; Walshe, A. Ring Opening Polymerisation of

Epoxides Catalysed by a Uranyl Aryloxide and Uranyl Chloride. *Chem. Commun.* **2012**, 48**,** 985 – 987.

(18) (a) Thuéry, P.; Harrowfield, J. Recent advances in structural studies of heterometallic uranyl-containing coordination polymers and polynuclear closed species. *Dalton Trans*. **2017**, 46, 13660-13667; (b) Andrews, M. B.; Cahill, C. L. Uranyl Bearing Hybrid Materials: Synthesis, Speciation, and Solid-State Structures. *Chem. Rev.* **2013**, 113, 1121–1136.

(19) See for example: (a) Kalaj, M.; Carter, K. P.; Savchenkov, A. V.; Pyrch, M. M.; Cahill, C. L. Syntheses, Structures, and Comparisons of Heterometallic Uranyl Iodobenzoates with Monovalent Cations. *Inorg. Chem*. **2017**, 56, 9156-9168; (b) Arnold, P. L.; Pecharman, A.-F.; Hollis, E.; Yahia, A.; Maron, L.; Parsons, S.; Love, J. B. Uranyl oxo activation and functionalization by metal cation coordination. *Nat. Chem.* **2010**, 2, 1056-1061. (c) Sarsfield, M. J.; Helliwell, M.; Raftery, J. Distorted Equatorial Coordination Environments and Weakening of UO Bonds in Uranyl Complexes Containing NCN and NPN Ligands. *Inorg. Chem.* **2004**, 43, 3170-3179; (d) Arnold, P. L.; Patel, D.; Blake, A. J.; Wilson, C.; Love, J.B, Selective Oxo Functionalization of the Uranyl Ion with 3d Metal Cations. *J. Am. Chem. Soc.* **2006**, 128, 9610-9611.

(20) See for example (a) Di Pietro, P.; Kerridge, A. U-O_{yl} Stretching Vibrations as a Quantitative Measure of the Equatorial Bond Covalency in Uranyl Complexes: A Quantum-Chemical Investigation. *Inorg. Chem*. **2016**, 55, 573-583; (b) Vallet, V.; Wahlgren, U.; Grenthe, I. Probing the Nature of Chemical Bonding in Uranyl(VI) Complexes with Quantum Chemical Methods. *J. Phys. Chem. A* **2012**, 116, 12373-12380.

(21) (a) Terencio, T.; Roithová, J.; Brandès, S.; Rousselin, Y.; Penouilh, M. –J.; Meyer M. A Comparative IRMPD and DFT Study of Fe^{3+} and UO_2^{2+} Complexation with N-Methylacetohydroxamic Acid, Inorg. Chem. 2018, 57, 1125−1135; (b) Kannan, S.; Kumar, M.; Sadhu, B.; Jaccob, M.; Sundararajan, Unusual intramolecular CH…O hydrogen bonding interaction between a sterically bulky amide and uranyl oxygen. M. *Dalton. Trans.* **2017**, 46, 16939-16946; (c) Watson, L.A.: Hay, B. P. Role of the Uranyl Oxo Group as a Hydrogen Bond Acceptor. *Inorg. Chem.* **2011**, 50, 2599-2605; (d) Fortier, S.; Hayton, T. W. Oxo ligand functionalization in the uranyl ion (UO_2^{2+}). *Coord. Chem. Rev.* **2010**, 254, 197-214.

(22) de Groot, J.; Cassell, B.; Basile, M.; Fetrow, T.; Forbes, T. Z. Charge-Assisted Hydrogen-Bonding and Crystallization Effects within U^{VI} Glycine Compounds. *Eur. J. Inorg. Chem.* **2017**, 1938–1946.

(23) See for example (a) Sather, A. C.; Berryman, O. B.; Rebek, Jr. J. Selective recognition and extraction of the uranyl ion from aqueous solutions with a recyclable chelating resin. *Chem. Sci.* **2013**, 4, 3601-3605; (b) Parker, B. F.; Knight, A. S.; Vukovic, S.; Arnold, J.; Francis M. B. A Peptoid-Based Combinatorial and Computational Approach to Developing Ligands for Uranyl Sequestration from Seawater. *Ind. Eng. Chem. Res.* **2016**, 55, 4187−4194; (b) Sather, A. C.; Berryman, O. B.; Rebek, Jr., J. Selective Recognition and Extraction of the Uranyl Ion. *J. Am. Chem. Soc.* **2010**, 132, 13572–13574; (c) Franczyk, T. S.; Czerwinski, K. R.; Raymond, K. N. Stereognostic Coordination Chemistry. 1. The Design and Synthesis of Chelators for the Uranyl Ion. *J. Am. Chem. Soc.* **1992**, 114, 8138-8146.

(24) (a) Kalaj, M.; Carter, K. P.; Cahill, C. L Isolating Equatorial and Oxo Based Influences on Uranyl Vibrational Spectroscopy in a Family of Hybrid Materials Featuring Halogen Bonding

Interactions with Uranyl Oxo Atoms. *Eur. J. Inorg. Chem.* **2017**, 4702-4713; (b) Carter, K. P.; Kalaj, M.; Surbella, R. G., III; Ducati, L. C.; Autschbach, J.; Cahill, C. L. Engaging the Terminal: Promoting Halogen Bonding Interactions with Uranyl Oxo Atoms. *Chem. Eur. J.* **2017**, 23, 15355-15369; (c) Surbella, R. G.; Ducati, L. C.; Pellegrini, K. L.; McNamara, B. K.; Autschbach, J.; Schwantes, J. M.; Cahill, C. L. Transuranic Hybrid Materials: Crystallographic and Computational Metrics of Supramolecular Assembly. *J. Amer. Chem. Soc*. **2017**, 139, 10843-10855; (d) Kalaj, M.; Carter, K. P.; Cahill, C. L.Utilizing bifurcated halogen-bonding interactions with the uranyl oxo group in the assembly of a UO_2-3-bromo-5-iodobenzoic acid coordination polymer. *Acta Crystallogr., Sect. B: Struct. Sci* **2017**, 73, 234-239; (e) Carter, K. P.; Kalaj, M.; Cahill, C. L. Harnessing uranyl oxo atoms via halogen bonding interactions in molecular uranyl materials featuring 2,5-diiodobenzoic acid and N-donor capping ligands. *Inorg. Chem. Front.* **2017**, 4, 65-78. (f) Carter, K. P.; Cahill, C. L. Combining coordination and supramolecular chemistry to explore uranyl assembly in the solid state. *Inorg. Chem. Front.* **2015**, 2, 141-156; (g) Deifela, N. P.; Cahill, C. L. *Chem. Commun*. **2011**, 47, 6114-6116.

(25) Surbella, R. G.; Cahill, C. L. The exploration of supramolecular interactions stemming from the $[UO_2(NCS)_4(H_2O)]^{2-}$ tecton and substituted pyridinium cations. *CrystEngComm* **2014**, 16, 2352-2364.

(26) Nuzzo, S.; Browne, M. P.; Twamley, B.; Lyons, M. E. G.; Baker, R. J. A structural and spectroscopic study of the first uranyl selenocyanate, $[Et_4N]_3[UO_2(NCSe)_5]$. *Inorganics*, 2016, **4**, 4-8.

(27) Rowland, C. E.; Kanatzidis, M. G.; Soderholm, L. Tetraalkylammonium Uranyl Isothiocyanates. *Inorg. Chem.* **2012**, 51, 11798-11804.

(28) (a) Qu, F.; Zhu, Q. –Q.; Liu, C. –L. Crystallization in Ionic Liquids: Synthesis, Properties, and Polymorphs of Uranyl Salts. *Cryst. Growth Des.* **2014**, 14, 6421−6432; (b) Aoyagi, N.; Shimojo, K.; Brooks, N. R.; Nagaishi, R.; Naganawa, H.; Van Hecke, K.; Van Meervelt, L.; Binnemans, K.; Kimura, T. Thermochromic properties of low-melting ionic uranyl isothiocyanate complexes. *Chem. Commun.* **2011**, 47, 4490–4492.

(29) Tamasi, A. L.; Rungthanapathsophon, P.; Dame, A. N.; Moody, M. A.; Barnes, C. L.; Wilkerson, M. P.; Walensky, J. R. Pseudo-halide uranyl salicylaldiminate complexes including the isolation of a rare uranyl azide. *J. Coord. Chem.* **2016**, 69, 1904-1913.

(30) Hashem, E.; Platts, J. A.; Hartl, F.; Lorusso, G.; Evangelisti, M.; Schulzke, C.; Baker, R. J. Thiocyanate Complexes of Uranium in Multiple Oxidation States: A Combined Structural, Magnetic, Spectroscopic, Spectroelectrochemical, and Theoretical Study. *Inorg. Chem.* **2014**, 53, 8624–8637.

(31) Down, A. W. The isolation of a salt of the tellurocyanate anion. *Chem. Commun.* 1968, 1290-1291.

(32) van der Waals radii taken from Alvarez, S. A cartography of the van der Waals territories. *Dalton Trans.* **2013**, 42, 8617-8636

(33) (a) Reddi, R.; Singarapu, K. K.; Pal, D.; Addlagatta, A. The unique functional role of the C–H···S hydrogen bond in the substrate specificity and enzyme catalysis of type 1 methionine aminopeptidase. *Mol. BioSyst.* **2016**, 12, 2408-2416; (b) Wei, K. J.; Ni, J.; Xie, Y. S.; Liu, Q. L. Solvent-induced 1- and 2-D Cd(II) coordination polymers based on a bent polypyridyl ligand. *Inorg. Chem. Commun.* **2007**, 10, 279–282; (c) Zhou, H. P.; Zhu, Y. M.; Chen, J. J.; Hu, Z. J.; Wu, J. Y.; Xie, Y.; Jiang, M. H.; Tao, X. T.; Tian, Y. P. A new ligand for the formation of a 3D structure

by significant C–H···S hydrogen bonds and π–π interactions. *Inorg. Chem. Commun.* **2006**, 9, 90–92; (d) Allen, F. H.; Bird, C. M.; Rowland, R. S.; Raithby, P. R. Hydrogen-Bond Acceptor and Donor Properties of Divalent Sulfur (Y-S-Z and R-S-H). *Acta Crystallogr. Sect. B Struct. Sci.* **1997**, 53, 696–701; (e) Desiraju, G. R.; Steiner, T. In The Weak Hydrogen Bond in Structural Chemistry and Biology, Oxford University Press **1999**.

(34) (a) Domagała, M.; Grabowski, S. J. Chemical Physics **2010**, 367, 1–6; (b) Domagała, M.; Grabowski, S. J. CH···N and CH···S Hydrogen Bonds Influence of Hybridization on Their Strength. *J. Phys. Chem. A* **2005**, 109, 5683-5688; (c) Scheiner, S.; Grabowski, S. J.; Kar T. Influence of Hybridization and Substitution on the Properties of the CH···O Hydrogen Bond. *J. Phys. Chem. A*, **2001,** 105, 10607-10612;

(35) (a) Biswas, S.; Ma, S.; Nuzzo, S.; Twamley, B.; Russell, A. T.; Platts, J. A.; Hartl F.;, Baker, R. J. Structural Variability of 4f and 5f Thiocyanate Complexes and Dissociation of Uranium(III)−Thiocyanate Bonds with Increased Ionicity. *Inorg Chem.* **2017**, DOI: 10.1021/acs.inorgchem.7b01560; (b) Collado, S.; Laca, A.; Díaz, M. Catalytic wet oxidation of thiocyanate with homogeneous copper(II) sulphate catalyst. *J. Hazard. Mater*. **2010**, 177, 183−189. (c) Kitanovski, N.; Golobič, A.; Čeh, B. Synthesis and Characterization of Mo(V)-oxido Complexes Containing the Thiocyanato-N Ligand. *Acta Chim. Slov*. **2008**, 55, 767-774; (d) Kirschenbaum, L. J.; Sun, Y. Reduction of the Tetrahydroxoargentate(111) Ion by Thiocyanate in Aqueous Alkaline Media. Inorg. Chem. 1991, 30, 2360−2365.

(36) Zalkin, A., Ruben, H.; Templeton, D. H. Structure of a new uranyl sulfate hydrate, α-$UO_2SO_4 \cdot 7H_2O$. *Inorg. Chem.* **1978**, 17, 3701–3702.

(37) Kampf, A.R., Plášil, J., Kasatkin, A.V., Marty, J.,Čejka, J., and Lapčák, L., Shumwayite, $[(UO_2)(SO_4)(H_2O)_2]_2 \cdot H_2O$, a new uranyl sulfate mineral from Red Canyon, San Juan County, Utah, USA. *Mineral. Mag.* **2017**, 81, 273-285.

(38) See for example: Michalczyk, R.; Schmidt, J. G.; Moody, E.; Li, Z.; Wu, R.; Dunlap, R. B.; Odom, J. D.; Silks III, L. A. Unusual C-H···Se=C Interactions in Aldols of Chiral N-Acyl Selones Detected by Gradient-Selected ^{1}H-^{77}Se HMQC NMR Spectroscopy and X-ray Crystallography. *Angew. Chem. Int. Ed.* **2000**, *39*, 3067-3070.

(39) (a) McKinnon, J. J.; Spackman, M. A.; Mitchell, A. S. *Acta Crystallogr. Sect. B: Struct. Sci.* **2004**, 60, 627; (b) Spackman, M. A. McKinnon, J. J. *CrystEngComm*, **2002**, 4, 378; (c) *CrystalExplorer* (Version 3.1), Wolff, S. K.; Grimwood, D. J.; McKinnon, J. J.; Turner, M. J.; Jayatilaka, D.; Spackman, M. A. University of Western Australia, **2012**.

(40) Qu, F.; Zhu, Q. –Q.; Liu, C. –L. Crystallization in Ionic Liquids: Synthesis, Properties, and Polymorphs of Uranyl Salts. *Cryst. Growth Des*. **2014**, 14, 6421-6432

(41) Jones, L. H.; Penneman, R. A. Infrared Spectra and Structure of Uranyl and Transuranium (V) and (VI) Ions in Aqueous Perchloric Acid Solution. *J. Chem. Phys.* **1953**, 21, 542-544.

(42) (a) Schnaars, D. D.; Wilson, R.E. Lattice Solvent and Crystal Phase Effects on the Vibrational Spectra of $UO_2Cl_4^{2-}$. *Inorg. Chem.* **2014**, 53, 11036−11045; (b) Schnaars, D. D.; Wilson, R.E. Structural and Vibrational Properties of $U(VI)O_2Cl_4^{2-}$ and $Pu(VI)O_2Cl_4^{2-}$ Complexes. *Inorg. Chem.* **2013**, 52, 14138−14147; (c) Herzberg, G. Infrared and Raman Spectra of Polyatomic Molecules. D. Van Nostrand Company, Inc, New York, 1946.

(43) Natrajan, L.S. Developments in the photophysics and photochemistry of actinide ions and their coordination compounds. *Coord. Chem. Rev.* **2012**, 256, 1583-1603.

(44) Redmond, M.P.; Cornet, S.M.; Woodall, S.D.; Whittaker, D.; Collison, D.; Helliwell, M.; Natrajan, L.S. Probing the local coordination environment and nuclearity of uranyl(VI) complexes in non-aqueous media by emission spectroscopy. *Dalton Trans*. **2011**, 40, 3914-3926.

(45) Hashem, E.; McCabe, T.; Schulzke, C.; Baker, R. J. Synthesis, Structure and Photophysical Properties of $[UO_2X_2(O{=}PPh_3)_2]$ (X = Cl, Br, I). *Dalton Trans.*, 2014, **43**, 1125-1131.

(46) Surbella III, R.G.; Andrews, M. B.; Cahill, C.L. Self-assembly of $[UO_2X_4]^{2-}$ (X=Cl, Br) dianions with γ substituted pyridinium cations: Structural systematics and fluorescence properties. *J. Solid State Chem*. **2016**, 236, 257-271.

(47) The ^{77}Se NMR chemical shift of Et_3NBzSe show no dependence on concentration, unlike Te···Te interactions which persist in solution, as shown by the concentration dependence of the ^{125}Te chemical shift. Elder, P. J. W.; Vargas-Baca, I. ^{125}Te NMR Provides Evidence of Autoassociation of Organo-Ditellurides in Solution. *Phys. Chem. Chem. Phys*. **2016**, 18, 30740-30747.

(48) Nakamoto, K. Infrared and Raman Spectra of Inorganic and Coordination Compounds, 4th Edn John Wiley & Sons.

(49) Carter, T. J.; Wilson, R. E. Coordination Chemistry of Homoleptic Actinide(IV)-Thiocyanate Complexes. *Chem. Eur. J.* **2015**, 21, 15575-15582.

(50) (a) Bleiholder, C.; Werz, D. B.; Köppel, H.; Gleiter, R. Theoretical Investigations on Chalcogen-Chalcogen Interactions: What Makes These Nonbonded Interactions Bonding? *J. Am.*

Chem. Soc. **2006**, 128, 2666-2674; (b) Bleiholder, C.; Gleiter, R.; Werz, D. B.; Köppel, H., Theoretical Investigations on Heteronuclear Chalcogen-Chalcogen Interactions: On the Nature of Weak Bonds between Chalcogen Centers. *Inorg. Chem.* **2007**, 46, 2249-2260.

(51) Guo, X.; An, X.; Li, Q. Se…N Chalcogen Bond and Se…X Halogen Bond involving F_2C=Se Influence of Hybridization, Substitution and Cooperativity. *J. Phys. Chem. A* **2015**, 119, 3518-3527.

(52) Alkorta, I.; Rozaz, I.; Elguero, J. Charge-Transfer Complexes between Dihalogen Compounds and Electron Donors. *J. Phys. Chem. A* **1998**, 102, 9278-9285.

(53) See for example (a) Mandal, A.; Patel, B. K.; Shuklaand, R.; Chopra, D. Impact of the complementary electronic nature of C–X and M–X halogens and intramolecular X···O interaction on supramolecular assemblies of Zn(II) complexes of o-halophenyl substituted hydrazides. *CrystEngComm* **2017**, 19, 1607–1619; (b) Farrell, D.; Kingston, S. J.; Tungulin, D.; Nuzzo, S.; Twamley, B.; Platts, J. A.; Baker, R. J. N-Aryl-9,10-phenanthreneimines as Scaffolds for Exploring Noncovalent Interactions: A Structural and Computational Study. *Eur. J. Org. Chem.* **2017**, 5597-5609.

(54) Duarte, D. J. R.; Sosa, G. L.; Peruchenaa, N. M.; Alkort, I. Halogen bonding. The role of the polarizability of the electron-pair donor. *Phys. Chem. Chem. Phys.* **2016**, 18, 7300—7309.

(55) See for example: Neel, A. J.; Hilton, M. J.; Sigman, M. S.; Toste, F. D. Exploiting non-covalent π interactions for catalyst design. *Nature*, **2017**, 543, 637.

(56) SHELXTL 6.14 Bruker AXS Inc., Madison, WI, 2000-2003; Sheldrick, G.M. *Acta Cryst.* **2008**, *A64*, 112-122.

(57) Momma, K.; Izumi, F. VESTA 3 for three-dimensional visualization of crystal, volumetric and morphology data. *J. Appl. Crystallogr*. **2011**, 44, 1272-1276.

(58) Zhao Y.; Truhlar, D. G. *Theor. Chem. Acc.,* **2008**, *120*, 215.

(59) Gaussian 09, Revision C.01, M. J. Frisch, G. W. Trucks, H. B. Schlegel, G. E. Scuseria, M. A. Robb, J. R. Cheeseman, G. Scalmani, V. Barone, B. Mennucci, G. A. Petersson, H. Nakatsuji, M. Caricato, X. Li, H. P. Hratchian, A. F. Izmaylov, J. Bloino, G. Zheng, J. L. Sonnenberg, M. Hada, M. Ehara, K. Toyota, R. Fukuda, J. Hasegawa, M. Ishida, T. Nakajima, Y. Honda, O. Kitao, H. Nakai, T. Vreven, J. A. Montgomery, Jr., J. E. Peralta, F. Ogliaro, M. Bearpark, J. J. Heyd, E. Brothers, K. N. Kudin, V. N. Staroverov, T. Keith, R. Kobayashi, J. Normand, K. Raghavachari, A. Rendell, J. C. Burant, S. S. Iyengar, J. Tomasi, M. Cossi, N. Rega, J. M. Millam, M. Klene, J. E. Knox, J. B. Cross, V. Bakken, C. Adamo, J. Jaramillo, R. Gomperts, R. E. Stratmann, O. Yazyev, A. J. Austin, R. Cammi, C. Pomelli, J. W. Ochterski, R. L. Martin, K. Morokuma, V. G. Zakrzewski, G. A. Voth, P. Salvador, J. J. Dannenberg, S. Dapprich, A. D. Daniels, O. Farkas, J. B. Foresman, J. V. Ortiz, J. Cioslowski, and D. J. Fox, Gaussian, Inc., Wallingford CT, **2010**.

(60) Küchle, W.; Dolg, M.; Stoll, H.; Preuss, H. Energy-adjusted pseudopotentials for the actinides. Parameter sets and test calculations for thorium and thorium monoxide. *J. Chem. Phys.* **1994**, 100, 7535.

(61) AIMAll (Version 12.06.03), Todd A. Keith, TK Gristmill Software, Overland Park KS, USA, 2012.

For ToC use only

Chalcogenide bonding within the coordination sphere of the uranyl ion have been explored using X-ray crystallography, vibrational and photoluminescence spectroscopy.

Chalcogenide interactions

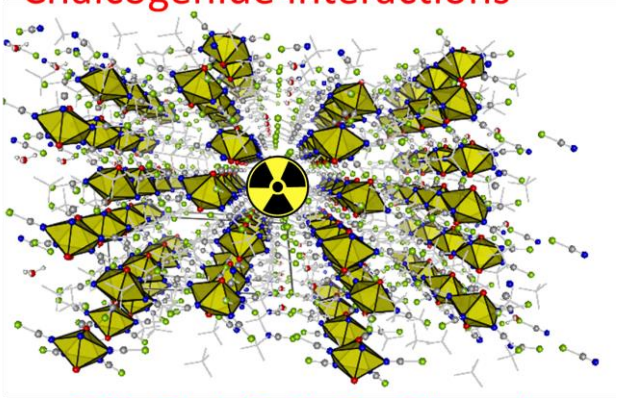

C-H···S(e)/C-H···O=U bonds